Performance Modelling of a Proton Exchange Membrane Fuel Cell

by

Curtis Lincoln Marr
B.Eng., University of Victoria, 1989

A Thesis Submitted in Partial Fulfillment of the
Requirements for the Degree of
MASTER OF APPLIED SCIENCE
in the
Department of Mechanical Engineering.

We accept this thesis as conforming
to the required standard

[redacted]

Dr. X. Li, Supervisor (Dept. of Mechanical Engineering)

[redacted]

Dr.N. Djilali, Departmental Member (Dept. of Mechanical Engineering)

[redacted]

Dr. M. Nahon, Outside Member (Dept. of Mechanical Engineering)

[redacted]

Dr. D. Harrington, External Examiner (Dept. of Chemistry)

Supervisor: Dr. X Li

Abstract

Automobile use has significantly increased the amount of urban air pollution. The amount of pollution can be reduced by introducing and encouraging the use of zero emission vehicles. The proton exchange membrane fuel cell (PEMFC) has strong potential as the power source for this type of transportation application. This thesis presents a one dimensional isothermal model of a proton exchange membrane fuel cell. The model is based on the work of Bernardi and Verbrugge and that of Weisbrod with additional formulation for electrical resistance in the plate and electrode, and some simplifications for gas transport processes.

Overall, the model predictions agree qualitatively with the known results. Analysis of the catalyst layer indicates that most of the electrochemical reaction occurs in the first few micrometers. This suggests that the catalyst is not being effectively used. The present model predicts effective use of Pt catalyst decreases with increasing current density, and hence, lower loadings of Pt are possible for higher current densities of practical interest without adverse effect on performance. Investigation into the optimum performance of the catalyst layer predicts an optimum value for void fraction of 60%. This value appears to be independent of current density. This model also predicts that there is an optimum value for surface area correction of the catalyst used. A 40% supported Pt catalyst is predicted to give the best performance amongst 20%, 40%, 60% and 80% supported Pt catalysts.

This model can be improved with two modifications to the formulation. Addition of two phase flow in all component models would improve quantitative predictions. In the catalyst layer, a more detailed model of catalyst layer composition would both improve quantitative predictions and point to other areas for optimisation.

Examiners:

[redacted]

Dr. X. Li, Supervisor (Dept. of Mechanical Engineering)

[redacted]

Dr.N. Djilali, Departmental Member (Dept. of Mechanical Engineering)

[redacted]

Dr. M. Nahon, Outside Member (Dept. of Mechanical Engineering)

[redacted]

Dr. D. Harrington, External Examiner (Dept. of Chemistry)

Table of Contents

List of Tables

List of Figures

Nomenclature

A - area

a - association factor of solvent

b - Tafel slope

C - concentration

ΔC - concentration change

d_h - hydraulic diameter of channel

D - diffusion coefficient

E - voltage potential

F - Faraday's Constant (96487 C/mole)

ΔG - Gibbs Free Energy (J/molK)

H - Henry's constant

h - height

I - current density

K - permeability

L - length of cell

l - length

M - molecular weight (g/mole)

m - mass loading of catalyst

N - molar flux

n - number of electrons transferred in reaction

n_g - number of grooves in channel (eq. [2.54]

PD_{ij} - pressure diffusivity product constant $(atm\ cm^2/s)$ of species i into j.

Pr - Prandtl number

p - pressure

Δp - pressure drop

R - resistance

$\bar{R}$ - universal gas constant 8.314 J/mol K

ΔS - change in entropy

S_0 - Sutherland constant

Sh - Sherwood number

T - temperature

V - volume

V_A - molal volume of the solute A at its normal boiling temperature

v - velocity

W - width of cell

w - width

x - mole fraction

Greek Symbols

α - transfer coefficient

δ - thickness

γ - reaction order

κ - conductivity

μ - viscosity

ψ - utilisation

ϕ - void fraction

ρ - resistivity

ξ - empirical constant

Subscripts

0 - standard reference value

i - species

a - anode

act - activation

A - solute

B - solvent

c - cathode

ci - critical value

ch - channel

E - electric

el - electrode

eff - effective value

f - fixed species

lm - logarithmic mean

me - membrane

p - pressure

pl - plate

ref - reference value

s - channel support

Acknowledgements

This work has been made possible with a grant from collaboration between British Gas Investments Canada, Ballard Power Systems and the National Science and Engineering Research Council of Canada.

I would like to thank my supervisor, Dr. Xianguo Li, and Dr. David Sanborn Scott for their invaluable help and guidance over the course of this thesis. Thanks should also go to Dr. Gunter Simader for his help and insight into fuel cells and electrochemistry.

I would also like to thank my family for their encouragement and support, Ian of Wine, Ian of Beer, my officemates, the outstanding group of people in IESVic, especially Dolores and Sue, the electrochemical gurus at SFU and UVic, Dr. Wu Sheng Lu, the Dalai Lama, and finally, the person who said "When the going gets tough, the tough get empirical."

So long, and thanks for all the fish!

Chapter 1

Introduction

The automobile of today is powered by an internal combustion engine, which runs by combustion of fossil fuels. However, combustion of fossil fuels is not a clean process and "increases fine particulates in the atmosphere, ground level ozone, and toxic substances [1, pg. 1]." As automobile use increases, the vehicular contribution to air pollution also increases. For example, in the suburban region of Vancouver, B.C., automobiles now account for 75% of air pollution [2].

As the level of air pollution in cities increases, so does concern over the health and environmental problems it causes. Although legislating tougher vehicular emission standards will reduce the net amount of emissions for each vehicle, this approach will be ineffective if the number of vehicles increases faster than the rate that emission controls can reduce emissions. In an effort to slow the amount of pollution produced by vehicles, both California and British Columbia have enacted legislation that encourages the production and use of zero emission vehicles, or ZEVs.

A ZEV is a vehicle which does not emit carbon or nitrogen compounds as waste products. Thus, its operation does not contribute to local air pollution. Several

technologies, including fuel cells and batteries, may be used to power a ZEV. Of these technologies, the proton exchange membrane fuel cell, or PEMFC, has very good potential to replace the internal combustion engine as the vehicular power train.

Although batteries are capable of powering a ZEV, they face many technical challenges. Perhaps the most difficult hurdle facing batteries is their low power to weight ratio. Because batteries are often composed of dense metals, it is very challenging to achieve high power densities. By contrast, the majority of the material used in a PEMFC is graphite. This material is very light by comparison, giving the PEMFC a higher power density [3, pg. 185] than conventional lead acid batteries.

While other types of fuel cells exist, there are several advantages that favour using PEMFCs for transportation. First, the PEMFC typically operates between 70 and 95°C. A low operating temperature allows PEMFCs to warm up quickly. By comparison, phosphoric acid, molten carbonate, and solid oxide fuel cells all operate at temperatures above 200°C [4]. Warm up time for these types of cells is much longer, making them unsuitable for applications in transportation.

Although alkaline cells operate in a temperature range similar to PEMFCs, they are susceptible to CO_2 impurities[3, pg. 277]. In an alkaline cell, CO_2 reacts with the alkaline electrolyte to form carbonates. These build up in the electrodes, and eventually prevent reactants from reaching the reaction sites. Because CO_2 does not react with PEM components, it is not necessary to remove the CO_2 before use, which allows PEMFC systems to operate without ancillary scrubbing devices.

Finally, the PEMFC uses a solid electrolyte. Fuel cells which use liquid electrolytes have more complications associated with their manufacture and operation. Liquid electrolytes leak, and cannot provide any structural support. Solid electrolytes do not have these problems, and consequently, ease the construction and eliminate the problem of corrosive electrolyte leakage in the cell.

On the other hand, the PEMFC is not without its own problems. Using a proton exchange membrane complicates water management [3, pg. 288]. The membrane has a tendency to dehydrate as current density increases. Membrane dehydration lowers the ability to conduct protons and consequently degrades cell performance. As a result, both fuel and oxidant streams must be humidified. Reactant humidification complicates PEMFC operation and lowers power density.

A PEMFC also is limited in its choice of catalysts. The acidic nature and low temperature of the PEMFC make it necessary to use noble metals as catalysts [3, pg. 281]. Noble metal catalysts are quite expensive, which puts PEMFCs at a cost disadvantage when compared to other types of cells that can use less expensive catalysts.

Further, the catalyst also is susceptible to carbon monoxide poisoning [3, pg. 277]. Carbon monoxide attaches itself to the catalyst sites, and prevents any other reaction from happening at these sites. As more sites are covered, the cell performance decreases. This susceptibility requires that PEMFC systems either scrub the H_2 stream, or use very clean sources of H_2.

Despite these technical hurdles, systems of PEMFCs have been successfully integrated into both buses [5] and vans [6]. However, PEMFC systems are significantly more expensive than both internal combustion engines and batteries. If PEMFCs are to become commercially viable, it is critical to reduce cost and increase power density through engineering optimisation, which requires a better understanding of PEMFCs and what parameters govern their performance. While prototyping and experimentation are excellent tools, they are expensive to implement and subject to practical limitations. Computer modelling is more cost effective, and easier to implement when changes in design are made.

In this thesis, a theoretical model will be formulated for the performance of a

single PEMFC, and the effect of various design and operating parameters on the cell performance will be investigated. In particular, catalyst loading optimisation will be investigated and the results will be presented.

1.1 Operational Principle of the PEMFC

A proton exchange membrane fuel cell (PEMFC) converts chemical energy of a fuel, such as H_2, and an oxidant, such as O_2, into electrical energy. It consists of two gas distribution plates and a membrane electrode assembly, or MEA. The MEA is composed of two electrodes and a proton conducting membrane. The MEA is constructed by applying a layer of catalyst in between each electrode and the membrane. The construction of MEAs typically involves pressing the components together under high pressure and temperature. This assembly is placed between the gas distribution plates. Figure 1.1 shows a schematic of a typical PEMFC.

When a load is connected between the two electrodes, the circuit is complete and electrons can flow from the anode to the cathode. For an ideal PEMFC, the overall cell reaction equation is

$$H_2 + \frac{1}{2}O_2 \longrightarrow H_2O + \text{electrical work} + \text{heat} \tag{1.1}$$

Hydrogen gas is fed into one of the gas distribution plates. It diffuses through an electrode, called the anode. At the anode, the electrochemical reaction occurs as follows:

$$H_2 \longrightarrow 2H^+ + 2e^- \tag{1.2}$$

The protons migrate through the membrane until they reach the catalyst layer at the boundary between the membrane and cathode. The electrons migrate through

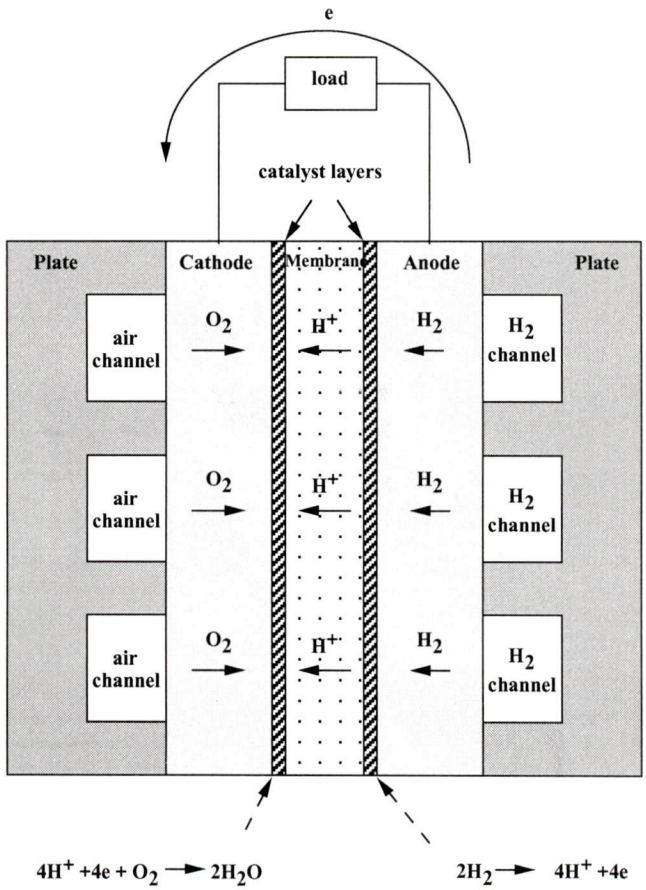

Figure 1.1: Cross sectional view of a typical PEMFC

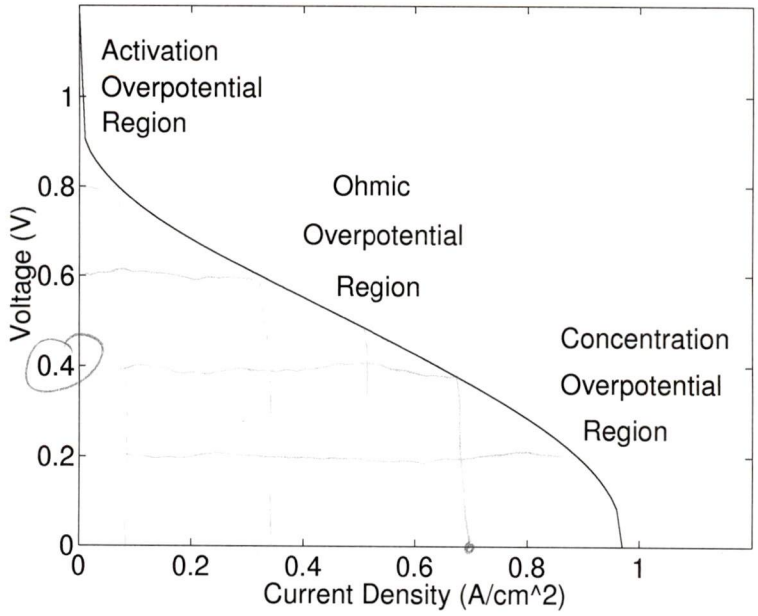

Figure 1.2: A typical polarisation curve characterising the performance of the PEMFC

the anode, through the load, and back to the other electrode, often referred to as the cathode.

Oxygen gas, whether pure or diluted (as in air), is fed through the other plate and diffuses through the cathode. When the O_2 molecules reach the catalyst layer, they react with the protons. The cathode reaction is

$$\frac{1}{2}O_2 + 2H^+ + 2e^- \longrightarrow H_2O \tag{1.3}$$

Because of irreversibilities, the voltage of the cell changes with the amount of current produced. A typical voltage current density curve, referred to as a polarisation plot, is shown in fig. 1.2. The polarisation curve is often broken into three regions: activation overpotential, ohmic overpotential, and concentration overpotential.

In the activation overpotential region, the dominant source of losses is due to resistance to electrochemical reactions. These losses, also referred to as activation

losses, occur when slow electrochemical reactions are driven from equilibrium in order to produce electric current. As the current drawn increases, the activation losses also increase.

In the ohmic overpotential region, activation losses increase at a slower rate than ohmic losses. In this region, losses from electric and ionic resistance in the cell are the most significant source of losses.

In the concentration overpotential region, losses due to mass transport limitations are dominant. Concentration overpotential occurs when the chemical reaction is limited by the rate at which reactants can be supplied. Starvation of reactants slow the electrochemical reaction, and lowers the potential of the cell. In this sense, the lack of reactants at the reaction sites essentially increases the resistance to the electrochemical reaction.

1.2 Objectives of the Thesis

The performance of a cell depends on the degree of activation, ohmic and concentration overpotentials. A simple, yet accurate, model to predict these losses would be very useful. It would enable one to understand the cell performance under different operating and design parameters, and point to directions for cell performance enhancements. This model should contain all the important fundamental processes occurring in the cell, be simple enough to have reasonable computational requirements such that it could be integrated into a larger stack model that would allow analysis of fuel cell systems.

Therefore, this thesis has the following objectives:

- to formulate and implement a computer model of PEMFC performance that

gives reasonable predictions with simplified fundamental, governing equations

- to investigate the performance effects of operating and design parameters
- to investigate electrochemical reaction and mass transport processes in the catalyst layer.
- to improve and optimise the utilisation of catalyst.

1.3 Review of Previous Work

Over the past decade, several different approaches have been used to model single PEMFC operation. The difference in approach can be roughly correlated to the level at which the model requires empirical parameters. Wholly empirical models rely almost entirely on experimental results and group some, if not all, of the physical processes into simple formulae. As models become more analytical, more fundamental equations are used to describe physical processes. Experimental data is replaced by physical properties.

A concise, empirical model of PEMFC performance was developed by Kim et al [7] at Texas A&M. Kim's model breaks the polarisation curve into a lumped set of parameters for electrochemistry, ohmic losses and concentration losses. The formulation is:

$$E = E_{oc} - b\log(I) - RI - m\exp(ni) \tag{1.4}$$

where E_{oc} is the open circuit voltage, b is the Tafel slope, I is the cell current, R is the internal resistance of the cell, and m and n are empirical constants used to fit data to the curve.

Although Kim's model is easy to fit to any polarisation curve, it does not give much insight to the relative contributions of specific fuel cell phenomena to the losses. It is not suitable as either a model or an initial framework on which to base a model.

Another empirical model was developed by Amphlett et al [8] at Royal Military College, Kingston. This model lumps the performance losses into parametric equations. The parameters were quantified by running experimental fits with a Ballard Mark IV (Nafion membrane) cell. This work was later extended to get parameters for a Ballard Mark V cell [9]. With this approach, the electrochemical and ohmic losses are consolidated into a set of ten parameters. The formulation for this model is:

$$\eta_{act} = \xi_1 + \xi_2 T + \xi_3 T[\ln(C_{O_2})] + \xi_4 T \ln(I) \tag{1.5}$$

$$R_{int} = \gamma_1 + \gamma_2 T + \gamma_3 i + \gamma_4 T i + \gamma_5 T^2 + \gamma_6 I^2 \tag{1.6}$$

where ξ_i, and γ_i are empirical parameters, I is the cell current in amperes, T is the cell temperature in Kelvin, and C_{O_2} is the catalyst surface concentration of O_2 in moles/cm^3.

While this model does account for changes in temperature and gas stream, it is not adequate for three reasons. First, the empirical parameters are dependent upon the cell that the measurements were taken from. This model would not give reliable information for a cell that had a different membrane, or had a different manufacture. Second, Amphlett's model merges many key parameters together. This makes it difficult to interpret the effects of changing physical properties (eg., electrode resistivity) in the cell. Finally, the model is valid only for low to mid current densities.

It has not been experimentally verified for current densities greater than 0.5 A/cm^2 [10].

Kim's and Amphlett's models use concise, simple expressions. However, they rely on empirically determined parameters which are dependent upon how the cell is configured or manufactured, and not on the physical properties associated with the configuration or manufacture of the cell. A more fundamental approach is needed.

Several semi-empirical models have been proposed by other groups of researchers. In general, the models follow a similar approach, but differ in the details associated with their assumptions. The general approach is to break the cell into an electrolyte, a catalyst layer, and a gas diffusor. While several other models exist [11, 12], the most widely known models have come from Bernardi and Verbrugge at General Motors [13, 14] and the researchers at Los Alamos National Laboratory [15, 16].

The model of Bernardi and Verbrugge [13, 14] uses fundamental equations for the different processes in a PEM cell. Seven differential equations are used to account for gas diffusion, water transport in the membrane, and electrochemistry. While the model is very comprehensive and forms an excellent template for a fuel cell model, it provides no details on modelling the electrical resistance in the plate and electrode. This model is also controversial because of some of its assumptions.

There are three questionable assumptions in the model. First, the models for mass transport in the cell assume plug flow, which is clearly not the case for a typical PEM cell. Second, the electrochemical assumptions do not give values that are observed experimentally. This model would give Tafel slopes of approximately 30 mV/decade, while experimental results range from 60 - 90 mV/decade [17, 16]. Finally, the water transport model for the membrane may be inaccurate. Hydraulic permeability, the parameter that models osmotic drag, may vary by two orders of

magnitude [14, pg. 2482], making it unreliable for calculating any mass balances. In addition, some questions about the charge conservation [10, pg. 23] assumptions for the membrane model have been raised.

The models developed at Los Alamos are predominantly empirical. Springer developed models for both water transport [15] and catalyst layer kinetics [16]. In these models, experimental data were taken and fitted to generic curves.

While these models are excellent, the empirical approach limits development within this model. The water transport model is only suitable for Nafion. The catalyst layer model [16] is also unusable because it is not flexible enough on its own to account for changes in catalyst loading and support changes.

Also at Los Alamos, Weisbrod [18] applied a more analytical approach to modelling the catalyst layer and integrated this with Springer's water transport model. Weisbrod modelled the electrochemistry with the Butler Volmer equation, and used empirical data for both the pressure-temperature dependencies of exchange current density and the Tafel slopes. This approach seems to be the best compromise so far between analytical and empirical models. In addition to modelling fuel cell behaviour, Weisbrod briefly discussed catalyst loading and optimisation. However, like Bernardi, Weisbrod does not provide any details for ohmic losses in the electrode, and assumes plug flow for the cell.

To summarise, the empirical models [7, 8] their performance predictions require that a set of measurements for each cell that needs modelling. Bernardi's model forms a good framework, but requires improvements in some portions of the model and some of the assumptions. Weisbrod's model provides an improved model of the catalyst layer, but it also lacks formulation for electrical conductivity of the plate and electrode.

Chapter 2

Model Formulation

The model presented in this thesis builds on the work of Bernardi and Weisbrod. The membrane model of Bernardi is combined with Weisbrod's catalyst layer model. While both these models use the Stephan-Maxwell equation for electrode gas diffusion, in this model, the Stephan-Maxwell equation is replaced with an engineering approximation. Further, approximations for the resistance of the plate and electrode are added.

The model breaks the cell into the following components: catalyst layer, membrane, electrode, gas distribution plate, and gas stream. The cell is analysed by starting with the basic reaction, and following the transport streams from the boundary of the catalyst layer to the inlet boundary of the gas stream.

The cell dimensions allow certain simplifications to be made. First, the model assumes steady state conditions. This is reasonable because most cell tests are conducted under these conditions. Second, because the thickness is small compared to the area of the cell, the model formulation can be reduced to one dimensional equations. Finally, the cell is assumed isothermal due to the relative thinness of the cell

and the ability of the cell materials to conduct heat.

Performance in the cell is modelled by taking the reversible cell voltage and subtracting the losses from it. This model breaks the losses into ohmic and activation losses, as given below,

$$E = E_r - \eta_{act} - \eta_{ohmic} \tag{2.1}$$

where E_r is the reversible voltage, η_{act} is the loss due to electrochemical reactions, and η_{ohmic} is the loss due to ohmic resistance.

2.1 Reversible Voltage Potential

For the fuel cell reaction described in eq. (1.1), an ideal cell potential is attained when the cell is at thermodynamic equilibrium. The reversible cell potential can be calculated with the Nernst equation [8]:

$$E_r = \frac{\Delta G}{2F} + \frac{RT}{2F}[\ln(p_{H_2}) + \frac{1}{2}\ln(p_{O_2})] \tag{2.2}$$

where ΔG is the change in Gibbs Free Energy, and the partial pressures of the reactant gases, p_{H_2} and p_{O_2}, use atm as units. The first term represents the reversible cell potential at standard temperature and pressure. The second term corrects for changes in gas pressures. To correct for changes in temperature, an additional term is added to the Nernst equation. The Nernst equation becomes

$$E_r = \frac{\Delta G}{2F} + \frac{\Delta S}{2F}(T - T_0) + \frac{RT}{2F}[\ln(p_{H_2}) + \frac{1}{2}\ln(p_{O_2})] \tag{2.3}$$

where ΔS is the change in entropy for each mole of fuel consumed. The temperature

of the cell, T, and the reference temperature, T_0, are in degrees K. Using standard values for Δ G and Δ S, eq. [2.3] reduces to [8]:

$$E_r = 1.229 - 0.85 \times 10^3(T - 298.15) + 4.31 \cdot 10^{-5} T \times [\ln(p_{h_2}) + \frac{1}{2}\ln(p_{o_2})] \quad (2.4)$$

where E_r is in volts, T is in degrees Kelvin, and p_{h_2} and p_{o_2} are in atm.

2.2 Catalyst Layer

The catalyst layer is situated between the electrode and membrane. In a typical PEMFC, the catalyst layer is composed of a porous mixture of platinum, often supported with a carbon substrate, ionomer (membrane material), and a Teflon (PTFE) binder. This region forms the heart of the fuel cell reaction and power production. The electrochemical reaction that occurs in the catalyst layer determines the performance of the cell.

For this model, the catalyst layer is set up as a one dimensional composition of catalyst particles interspersed between the membrane and electrode. Figure 2.1 shows how the catalyst layer is formed. Fluxes are considered positive in the positive z direction.

The cathode catalyst layer is the most complex region to model in the cell. The most important quantities to calculate are the losses due to electrochemical overpotential and ionic resistance. However, to calculate these values, it is necessary to account for the electrochemical reaction, diffusion through the layer, as well as ionic losses. There are several different coupled processes at work.

At the cathode layer boundaries, reactant gas diffuses from the electrode, while ions migrate from the membrane. Inside the catalyst layer,O_2 reacts with protons and

electrons on the catalyst surface. Protons and O_2 react to form H_2O. The cathode reaction is

$$\tfrac{1}{2}O_2 + 2H^+ + 2\bar{e} \longrightarrow 2H_2O$$

At the anode boundaries, H_2 diffuses from the electrode and protons and electrons migrate away. Within the anode catalyst layer, the electrochemical reaction produces protons and electrons from H_2 molecules. The anode reaction is

$$H_2 \longrightarrow 2H^+ + 2\bar{e}$$

2.2.1 Electrochemistry

The classical form of the Butler-Volmer equation [19, pg. 103] is shown in equation [2.5]. This equation describes the relationship between current density and overpotential for a single step electrochemical reaction.

$$I = I_0 \left[\exp\left(\frac{-\beta n F \eta}{RT}\right) - \exp\left(\frac{(1-\beta)\, nF\eta}{RT}\right)\right] \tag{2.5}$$

The exchange current density, I_0 is a measure of the amount of electrochemical activity that takes place at the reaction site. The symmetry factor, β, indicates how easily a reaction proceeds in one direction. The number of electrons, n, refers to the electrons transferred reaction.

However, the symmetry factor is only applicable for a simple single step reaction. In a PEMFC, the reactions are comprised of multistep reactions. Within a multistep reaction, the overall reaction rate is limited by the slowest reaction rate. This step, called the rate determining step, can be difficult to determine analytically. For multistep reactions, eq. [2.6] is used

$$I = I_0 \left[\exp\left(\frac{\alpha_a F \eta}{RT}\right) - \exp\left(\frac{(-\alpha_c F \eta}{RT}\right) \right] \tag{2.6}$$

where α_a and α_c are the anodic and cathodic transfer coefficients. The Tafel slope is defined as

$$b = \frac{\delta \eta}{dlogI} \tag{2.7}$$

and related to the transfer coefficient with the following formula.

$$b = 2.303 \frac{RT}{\alpha F} \tag{2.8}$$

With values for Tafel slope and exchange current density, the overpotential for a given current density can be calculated. The values of α and I_0 for each reaction are discussed in the following sections.

H_2 Reaction

The reaction at the anode is relatively uncomplicated. A likely mechanism for H_2 evolution is the Tafel-Volmer mechanism[20]. This involves the following steps.

$$H_2 + 2M \longrightarrow 2MH$$

$$2MH \longrightarrow 2M + 2H^+ + 2\bar{e}$$

The Tafel slope is approximately 120 mV/decade at 20 C. Assuming a temperature dependent Tafel slope, the value of α would be approximately 0.5.

The exchange current density for this reaction in H_3PO_4 is 0.021 A/cm^2 at 303 K and 0.173 A/cm^2 at 576 K [21]. Assuming the exchange current density is the same for Nafion, the exchange current density was approximated linearly with the empirical relationship

$$I_0 = 0.00109(T - 273.15) \tag{2.9}$$

Electrode	α	exchange current density
anode	0.5	$I_0 = 0.00109(T - 273.15)$
cathode	1.0	$\log_{10}(I_0) = 3.507 - \frac{4001}{T}$

Table 2.1: Electrochemical parameters

where the temperature is given in degrees Kelvin, and the exchange current density in A/cm^2.

O_2 Reaction

The O_2 mechanism is much more complicated and not yet well understood [22]. For this reaction, Tafel slopes of 60 - 70 mV [23] have been observed. Assuming that the rate determining step is irreversible [23], and that there is a one electron transfer, the value of α is 1.0.

The exchange current density data for O_2 in Nafion was taken from experiments by Parthasarathy [23]. The data were fitted with eq. (2.10) with an r^2 value of 0.977.

$$\log_{10}(I_0) = 3.507 - \frac{4001}{T} \tag{2.10}$$

Table 2.1 shows the electrochemical parameters that are used in this model.

Area Correction Factor

The catalyst in the layer is not a flat surface, but a collection of particles. The area correction factor represents the amount of surface area in a given volume of catalyst. If the thickness of the layer and the amount of catalyst are known, the area correction factor, A_v, can be calculated with the following relationship.

Catalyst Type	Area/load (m^2/g)
10%	140
20%	112
30%	88
40%	72
60%	32
80%	11
Pt black	28

Table 2.2: Surface Areas for different catalyst types

$$A_v = \frac{m_{Pt}\, A_s}{\delta_{cl}} \tag{2.11}$$

where A_s is the surface area per unit load (cm^2/gram), δ_{cl} is the thickness of the catalyst layer (cm) and m_{Pt} is the mass loading of Pt per unit area (mg/cm^2). Surface area varies greatly between different types of supported catalysts and Pt black. Values used for this model are shown in Table 2.2 [24].

Modification of Butler Volmer Equation

The Butler Volmer equation is further modified to allow for corrections from an experimentally derived reference point. The following relation [14] is used to scale the values.

$$I_0 = I_{0ref} \left(\frac{C}{C_{ref}} \right)^{\gamma} \tag{2.12}$$

where γ is the reaction order, I_{0ref} is a reference exchange current density, and C_{ref} is the reference concentration of reactant. Combining eq. [2.12] and eq. [2.5] gives the relationship for current density and overpotential. This gives the following relationship.

$$I = A_v I_{0ref} \left(\frac{C_{O_2}}{C_{O_2 ref}} \right)^{\gamma} \left[\exp\left(\frac{\alpha_a F \eta_{cl}}{RT} \right) - \exp\left(\frac{-\alpha_c F \eta_{cl}}{RT} \right) \right] \tag{2.13}$$

For the cathodic reaction, this model uses a reaction order of one [17], and a reference O_2 concentration of $1.2 \times 10^{-}6$ moles/cm^3 .

2.2.2 Void Fraction

Both the effective ionic conductivity, κ_{eff}, and the effective diffusion coefficient, D_{eff}, are dependent upon ϕ, the void fraction. The void fraction can be calculated from the platinum loading, the type of catalyst support, and the estimated thickness of the catalyst layer.

First the volume of the carbon is determined from the platinum load, and the type of carbon support.

$$V_C = \frac{(1 - \%Pt)\, m_{Pt}}{\%Pt\ \rho_C} \tag{2.14}$$

where m_{Pt} is the mass of Pt /cm^2 and %Pt is the percentage of Pt in the catalyst support. The volume occupied by the catalyst and support is

$$= \left(\frac{1}{\rho_{Pt}} + \frac{1 - \%Pt}{\%Pt\ \rho_C} \right) m_{Pt} \tag{2.15}$$

The ratio of catalyst thickness to layer thickness gives the percentage of space occupied by the catalyst in the layer.

$$= \frac{V_{catalyst}}{V_{layer}} \tag{2.16}$$

Because m_{Pt} is expressed as a load per surface area, the catalyst volume can be expressed as (thickness)$\times$ (surface area). By dividing both top and bottom by the unit area, the void fraction can be estimated as

$$\phi = 1 - \frac{\delta_{catalyst}}{\delta_{layer}} \tag{2.17}$$

2.2.3 Mass Diffusion

The effective diffusion coefficient, D_{eff} is dependent upon gas composition and the thickness and composition of the catalyst layer. At the present time, the physical composition of the catalyst layer is not well known, and more detailed study of the layer is needed to calculate this number.

Assuming the catalyst layer is 100% flooded and the ionomer has a similar diffusion coefficient to that of liquid water, the diffusion value, D_{ij}, is the diffusion coefficient for the gas species in liquid water. This value is temperature dependent and calculated using empirical methods. The Wilke Chang estimation [25, pg. 567] is used to approximate the change in D_{ij}:

$$D_{ij} = 7.4 \times 10^{-8} \frac{(aM_b)^{1/2}T}{\mu_b V_a{}^{0.6}} \tag{2.18}$$

where D_{ij} is the diffusion coefficient of species i into j (cm^2/s), M_b is the molecular weight of solvent (g/mole), μ_b is the viscosity of solvent (cP), T is the absolute temperature (K), V_a is the molal volume of the solute A at it's normal boiling temperature, and a is the association factor of solvent.

For V_a, values of 14.3 for H_2 and 25.6 for O_2 [25, pg. 58] are used. Using water as the solvent, the value of the association factor is 2.6 [25, pg. 588]. The viscosity of water is calculated with the empirical formula [26, pg. 701] given below.

$$ln\frac{\mu}{\mu_0} = -1.704 - 5.306z + 7.003z^2 \tag{2.19}$$

where

$$z = \frac{273}{T} \tag{2.20}$$

and the reference viscosity μ_0, is equal to $1.788 \times 10^{-3} kg/(ms)$.

The diffusion coefficient must correct for the porous nature of the catalyst layer. Following the approach of Bernardi [13] and Baumert [8], the product of the Bruggeman correction factor [27] and the bulk diffusion value is used to estimate the effective diffusion coefficient in the catalyst layer. This expression is described by eq. [2.21].

$$D_{eff} = \phi^{3/2} D_{ij} \tag{2.21}$$

2.2.4 Ionic Conductivity

The effective ionic conductivity of the catalyst layer, κ_{eff}, is dependent upon the catalyst layer composition. Because the layer composition is not known, ionic conductivity was modelled with a simple, empirical equation. Following the approach of Weis [18], porosity correction for conductivity is modeled with the following relationship:

$$\kappa_{eff} = \phi^2 \kappa_{bulk} \tag{2.22}$$

where κ_{eff} is the effective conductivity, ϕ is the void fraction and κ_{bulk} is the conductivity of bulk material.

Solubility

At the boundary of the catalyst layer, O_2 gas must first dissolve into the water in the catalyst layer. The solubility of O_2 gas in liquid water is calculated using Henry's constant. Assuming rapid saturation at the interface, the concentration at the boundary is

$$C_{O2} = \frac{p_{O2}}{H_{O2}} \tag{2.23}$$

where C_{O2} is the concentration of gas in liquid water (moles/cm^3), p_{O2} is the partial pressure of O_2 and H_{O2} is Henry's constant for oxygen in liquid water.

For a temperature dependent calculation, Henry's constant is fitted empirically with the following relationship [14, pg. 2482]:

$$\ln(H_{O2}) = -\frac{666}{T} + 14.1 \tag{2.24}$$

where T is the temperature in Kelvin units.

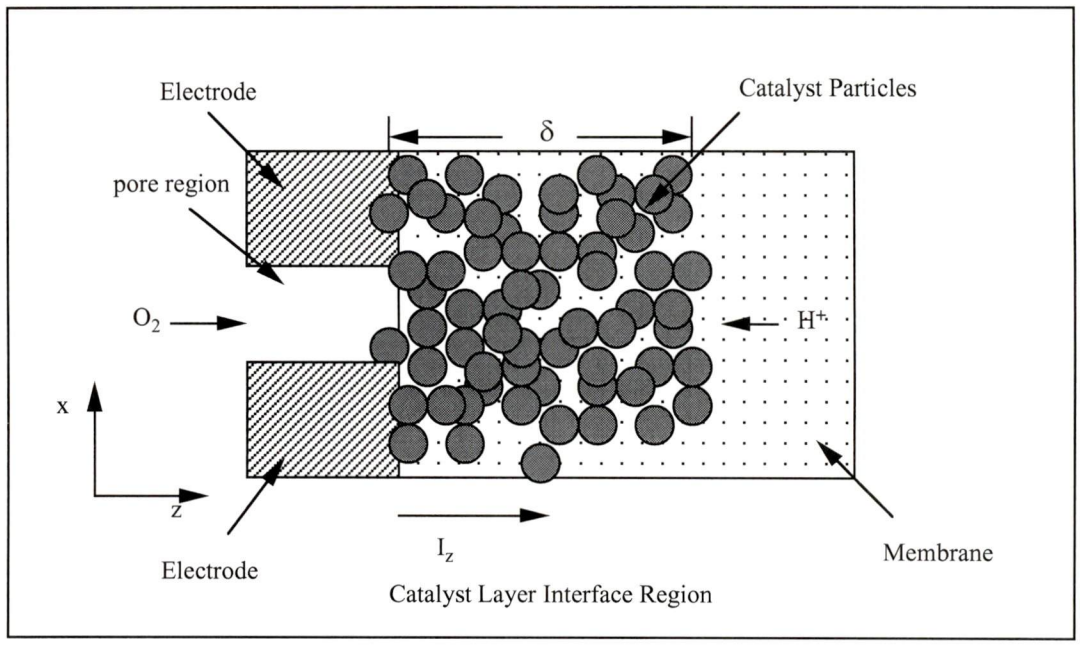

Figure 2.1: Diagram of a flooded cathode catalyst layer

2.2.5 Mathematical Formulation of the Catalyst Layer

The catalyst layer is modeled with a set of coupled differential equations and solved numerically. This model follows the work of Weisbrod, Grot and Vanderborgh [18] at Los Alamos National Laboratory. Their approach uses four one dimensional, coupled differential equations. The four equations used are:

$$\frac{dI_z}{dz} = A_v I_{0ref} \left(\frac{C_{o2}}{C_{o2ref}}\right) \left[\exp\left(\frac{\alpha_c F \eta_{cl}}{\bar{R}T}\right) - \exp\left(\frac{-\alpha_a F \eta_{cl}}{\bar{R}T}\right)\right] \tag{2.25}$$

$$\frac{d\eta_{cl}}{dz} = \frac{I_z}{\kappa_{eff}} \tag{2.26}$$

$$\frac{dN_{O2}}{dz} = -\frac{1}{4F}\frac{dI_z}{dz} \tag{2.27}$$

$$\frac{dC_{O2}}{dz} = -\frac{N_{O2}}{D_{O2}^{eff}} \tag{2.28}$$

where I_z is the ionic current, η_{cl} is the overpotential (a positive overpotential drives the cathodic current) , N_{O_2} is the molar flux of oxygen, and C_{O_2} is the concentration of oxygen.

Equation [2.25] models the electrochemical reaction in the catalyst layer. The second equation, eq. [2.26] accounts for the electrical conductivity of the catalyst layer. The molar flux necessary to balance the electrochemical reaction is modelled with equation [2.27]. The final differential equation, eq. [2.28], models the diffusion of reactant species within the catalyst layer.

For these four equations, four boundary conditions are needed. Given that the current density at the electrode boundary is equal to zero, the current density at the membrane boundary must be equal to the output current density of the cell. This gives the following boundary conditions. At z = 0,

$$I_z = 0 \tag{2.29}$$

and at z = δ,

$$I_z = I_\delta \tag{2.30}$$

For continuity, the concentration of O_2 at the electrode boundary, z = 0, must be:

$$C_{O2} = C_{O2}(0) \tag{2.31}$$

and, to for mass conservation at z = 0:

$$N_{O2} = \frac{I_\delta}{4F} \tag{2.32}$$

Mathematical Simplification of the Catalyst Layer

Because the mole flux equation, eq. [2.27] is a scalar adjustment of the current equation, integration of equ. [2.27] will give a value for N_{O_2}, which can be substituted into eq. [2.28]. This reduces the four original equations to three equations of the form:

$$\frac{dI_z}{dz} = A_v I_{0ref} \left(\frac{C_{o2}}{C_{o2ref}}\right) \left[\exp\left(\frac{\alpha_c F\eta}{RT}\right) - \exp\left(\frac{-\alpha_a F\eta}{RT}\right)\right] \tag{2.33}$$

$$\frac{d\eta}{dz} = \frac{I_z}{\kappa_{eff}} \tag{2.34}$$

$$\frac{dC_{O2}}{dz} = \frac{1}{4F D_{O2}^{eff}}(I_z - I_\delta) \tag{2.35}$$

After removal of the mole flux equation and its associated boundary condition, the three remaining conditions are:

At z = 0:

$$I_z = 0 \tag{2.36}$$

$$C_{O2} = C_{O2}(0) \tag{2.37}$$

and at z =δ:

$$I_z = I_\delta \tag{2.38}$$

2.3 Membrane

The membrane is situated between the anode and cathode catalyst layers. When an electric field is applied across the membrane, ions will migrate from one side to the other. The membrane allows ion migration, but prevents electron migration.

The membrane is a solid electrolyte. It consists of a backbone of flourinated carbon chains which has negatively charged sulfonates (SO_3^-) attached to it. These sites allow protons to jump from charge to charge to cross the membrane. Because the membrane is an electronic insulator, electrons are not able to cross the membrane.

Two approaches to the membrane model were examined for suitability. Bernardi and Verbrugge [14] used an analytical method to model the membrane. Springer et al [15] used empirical data and curve fitted these data to model the Nafion membranes. Because Bernardi's approach can model both Dow and Nafion, while Springer's model is limited to Nafion, this model uses the Bernardi approach for the membrane.

The membrane was modelled by following the approach of Bernardi and Verbrugge [13]. This approach uses the Nernst-Planck equation [13] calculates the ionic flux in the membrane. The Nernst-Planck equation is

$$N_i = -n_i \frac{F}{RT} D_i C_i \nabla E - D_i \nabla C_i + C_i v_i \tag{2.39}$$

where ∇E is the electric field across the membrane,∇C_i is the concentration gradient of mobile species across the membrane, v_i is the velocity of species i, C_i is the concentration of mobile species i, D_i is the diffusion coefficient of mobile species i, and n_i is the number of electric charges/mobile species i.

The three terms in this equation represent the molar flux due to the presence of an electric field, the flux due to concentration gradients, and the flux due to convection. Assuming the membrane is 100% wetted, the concentration gradient term will be zero and can be eliminated from the equation.

To preserve charge neutrality,

$$n_f C_f + n_i C_i = 0 \tag{2.40}$$

The charge concentration can be calculated from the concentration of fixed charge, C_f, and the number of fixed charges/species. Knowing that the number of fixed charges/species in this case is -1, the charge concentration is

$$C_{H^+} = -C_f \tag{2.41}$$

Defining the conductivity of the membrane as

$$\kappa = \frac{F^2 C_{H^+} D_{H^+}}{RT} \tag{2.42}$$

Setting I = FN_i and rearranging to solve for voltage drop, the Nernst-Planck equation reduces to

$$\nabla E = -\frac{I}{\kappa} + \frac{F}{\kappa} C_{H^+} v_i \tag{2.43}$$

Following the approach of Bernardi [13], the Schlogel equation is used to estimate the velocity of a water molecule within the membrane.

$$v = \frac{K_E}{\mu} n_f C_f F \nabla E - \frac{K_p}{\mu} \nabla p \tag{2.44}$$

where ∇E electric field across the membrane, ∇p_i is the pressure gradient across the membrane, K_p is the hydraulic permeability, K_E is the electric permeability and μ is the viscosity of liquid water. Rewriting the Shlogel equation as

$$v = -\frac{K_E}{\mu} C_{H^+} F \nabla E - \frac{K_p}{\mu} \nabla p \tag{2.45}$$

substituting into the Nernst Planck equation gives

$$\nabla E = -\frac{I}{\kappa} - \frac{F}{\kappa} c_{H^+} \left(\frac{K_E}{\mu} C_{H^+} F \nabla E + \frac{K_p}{\mu} \nabla p \right) \tag{2.46}$$

Parameter	Nafion	Dow
$\delta_m(\mu\text{m})$	220	175
c_{H+} (mol/cm^3)	$1.2 \cdot 10^{-3}$	$1.5 \cdot 10^{-3}$
K_E (cm^2)	$7.18 \cdot 10^{-16}$	$1.13 \cdot 10^{-15}$
K_p (cm^2)	$1.8 \cdot 10^{-14}$	$1.8 \cdot 10^{-14}$

Table 2.3: Membrane Properties

Rearranging the terms gives

$$\nabla E \left(1 + \frac{F^2 K_E C_{H+}^2}{\mu\kappa}\right) = -\left(\frac{I}{\kappa} + \frac{K_p}{\mu}\nabla p\right) \tag{2.47}$$

Reducing to a one dimensional equation and integrating gives

$$\Delta E = \delta_m \frac{(\frac{I}{\kappa} + \frac{FK_p\Delta p}{\kappa\mu\delta_m})}{(1 + \frac{F^2 K_E C_{H+}^2}{\mu\kappa})} \tag{2.48}$$

where ΔE drop in voltage across the membrane, and δm thickness of membrane. Table 2.3 shows the property values [14] used in this model for both Nafion and Dow membranes.

2.4 Electrode

The electrode collects the current produced at the catalyst layer while simultaneously diffusing gas reactants to the catalyst layer. In a PEM cell, the electrode is typically made of carbon cloth or carbon fiber paper. It is often impregnated with PTFE for both mechanical strength and water repelling properties.

Both gas transport and ohmic losses are accounted for in the electrode model. Flooding of the electrode is not modelled in any detail, due to the complex behaviour of flow in hydrophilic, porous media. Gas transport through the electrode is modelled

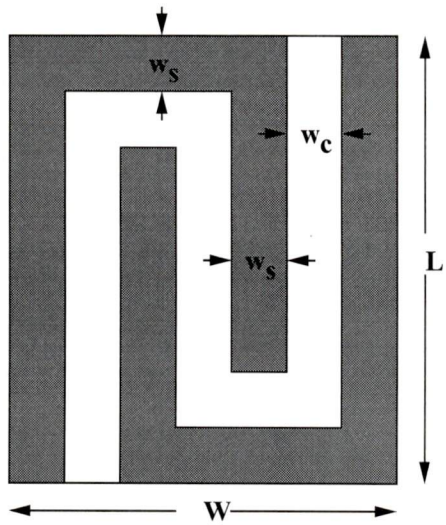

Figure 2.2: Top view of channel showing how dimensions are defined for calculating channel surface area

with a conventional Fick's Law equation that corrects for diffusion through porous media. The electric resistance losses are modelled with Ohm's law.

Fig. 2.2 shows how the channel is constructed in the cell. The area exposed to the electrode is defined as the length of the channel multiplied by the channel width.

The length of the channel is derived by setting the length of the channel in the direction of W equal to the total width minus the width of the end supports and the width of the channel. The length is measured from the center of the channel. For the distance in the W direction

$$l_w = W - (2w_s + w_{ch}) \tag{2.49}$$

where W is the width of the cell, l_w is the length of the channel in the W direction, and w_s and w_{ch} are the widths of the support and channel.

The channel length in the L direction is more complicated because the inlets and outlets are different lengths than the inner channels. The length of the inlet or

outlet is:

$$l_{outer} = L - (w_s + \frac{1}{2}w_{ch}) \tag{2.50}$$

where L is the length of the cell. The length of an inner channel is

$$l_{inner} = L - (2w_s + w_{ch}) \tag{2.51}$$

and the total distance in the L direction is:

$$l_l = l_{inlet} + l_{outlet} + (n_g - 2)l_{inner} \tag{2.52}$$

$$l_l = n_g L - (n_g - 1)(2w_s + w_{ch}) \tag{2.53}$$

Summing up the total for both width and length gives:

$$l_t = n_g(L - (2w_s + w_{ch})) + W \tag{2.54}$$

For the second group of terms, it is assumed that w_s is the same distance with respect to both length and width. Ohmic resistance is assumed constant within the temperature range 300-370 K and diffusion is assumed to spread O_2 evenly throughout the electrode surface such that there is a constant O_2 concentration at the electrode-catalyst layer interface.

2.4.1 Mass Transport

Reactants must diffuse through the electrode to reach the catalyst layer. Other models [8, 14, 16] use a Stephan Maxwell approximation to model the diffusion. This model uses an engineering approximation to reduce the amount of formulation needed to model the gas diffusion. For mass diffusion:

$$N = \frac{D_{ibulk} A_{ch}}{\delta_e} \Delta C_i \tag{2.55}$$

where ΔC_i is the concentration change of reactant i, ϕ is the void fraction of porous media, A_{ch} is the area of electrode exposed to flow channel, D_{ibulk} is the bulk diffusion rate of species i and N is the molar flow rate

To simulate the effect of porous media, Bernardi and Amphlett used a Bruggeman correction[15, pg. 2336]. The effective diffusion is given below.

$$D_{eff} = \phi_e^{3/2} D_{ibulk} \tag{2.56}$$

As mentioned in the previous section, the current density at the catalyst layer is assumed to be constant and independent of the flow geometry. It is also assumed that all the catalyst surface is active, and only the area in contact with the channel can diffuse reactant gas. Figure 2.3 shows a cross section of this diffusion pattern. With this assumption, the surface area exposed to the channel acts as a limit for mass diffusion. This intended to be a first step towards accounting for the non-uniformity of diffusion through the electrode due to the plate configuration. In the future, a correlation to relate the two dimensional diffusion to the cross-sectional configuration should be developed.

The gas diffusion current limit is estimated using the mass transport relation above. Assuming there are no other gradients besides the concentration gradient, the maximum molar flux that can be obtained occurs when the catalyst layer concentration is set to zero. The maximum current relationship becomes important when predicting performance in the concentration polarisation region.

$$N = \frac{D_{eff} A_{ch}}{\delta_e} C_s \tag{2.57}$$

where C_s concentration of reactant on the electrode surface

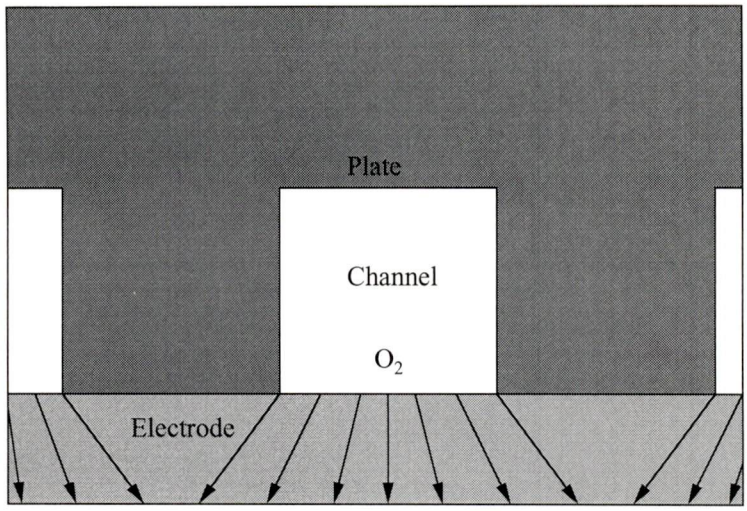

Figure 2.3: Diffusion from channel to catalyst layer surface

2.4.2 Electrode Resistance

It is difficult to develop an analytical equation for electrode resistance because of the asymmetrical nature of the problem. The formula presented here is an approximation meant only to get a reasonable value for the resistance in the electrode. If more accurate values are required, it will be necessary to compute these values based on simulations with an electronics or finite element software package.

The electrode resistance is derived by first assuming a constant current density in both the electrode and the reaction surface. Then it is assumed that the electrons take the shortest path from the reaction. From constant current density on the reaction surface, we assume that the average distance travelled into the x plane is one quarter of the width of the channel. By assuming constant current density at the plate/electrode interface, the average distance travelled will increase by $w_s/4$. Using

the basic equation for resistance in a slab:

$$R = \frac{\rho L}{A} \tag{2.58}$$

where R is the resistance of the slab, ρ is the resistivity of the material, L is the length of the block, and A is the cross sectional area of the block. If the cross sectional area is

$$A = \delta_{el} L_p \tag{2.59}$$

where δ_{el} is the thickness of the electrode and the mean path length is

$$L_p = \frac{1}{4}(w_{ch} + w_s) \tag{2.60}$$

then the average resistance in the electrode is

$$R = \frac{\rho(w_{ch} + w_s)}{4\delta_e L_p} \tag{2.61}$$

This is the resistance for only one side of the channel. For the entire electrode, there are $2n_g$ resistors in parallel. Thus

$$R_e = \frac{R}{2n_g} \tag{2.62}$$

$$R_e = \frac{\rho}{8n_g\delta_{el}L_p}(w_{ch} + w_s) \tag{2.63}$$

The cross sectional area is $\delta_e L_p$. Although not exact, this cross sectional area should give a reasonable approximation since the aspect ratio of channel width to electrode thickness is large. The resistivity is modeled with Bruggeman's correction. This correlation was developed for non-conducting spheres in a conducting medium [27], which is similar to the conditions in an electrode. Because there was not too significant of an effect by shape, this correlation was used. The porosity corrected resistivity of the electrode is

$$\rho_{eff} = \frac{\rho_{bulk}}{\phi^{3/2}} \tag{2.64}$$

Table 2.4 shows the values used for the base case electrode model.

Parameter	anode	cathode
L (mm)	50	50
W (mm)	50	50
δ_{el}* (mm)	0.25	0.25
ϕ **	0.4	0.4
ρ_{eff} * (Ωm)	60×10^{-6}	60×10^{-6}

* Ballard Power Systems [28].
** Bernardi [29].

Table 2.4: Electrode properties

2.5 Gas Distribution Plate

In a typical plate and frame PEM cell, the gas distribution plate is a plate of graphite with a serpentine flow channel cut into it. This channel is used to deliver reactants to the electrode and to collect current from the electrode. Two different phenomena are modelled in the plate:

- mass transport in the flow channel
- electric resistance in the plate

2.5.1 Channel flow

Many models [14, 15, 8] use a plug flow assumption to model mass diffusion to the electrode surface. Making this assumption effectively ignores the convective effect on mass transport in the channel.

In this model, mass transport is approximated using dimensionless parameters. A Sherwood number approximation [30] is used to estimate the amount of reactant that migrates from the bulk of the stream to the surface of the electrode.

This equation is valid for binary systems. Unmodified, a Sherwood number approximation would not be valid for a humidified air stream because this stream constitutes a ternary system. To overcome this complication, the air stream is reduced to a binary system of oxygen/bulk mixture of H_2O and N_2 by using a bulk diffusion correction [31]. A complete description of how diffusion coefficients are calculated is given in the gas properties section.

It is assumed that there is a constant concentration of O_2 at the electrode surface. Additionally, inlet and secondary flow patterns at the corners of the channel were ignored. These assumptions will give more conservative predictions because adding in correlations for inlet and flow around the corners would increase the mass transfer rate. The mass transport equation has the form

$$N = \frac{ShD_{ibulk}A_{ch}}{d_h}\Delta C_{ln} \tag{2.65}$$

where N is molar flow rate and ΔC_{ln} is the logarithmic average of concentration change between bulk gas concentration and electrode surface. The exposed area of the electrode on the channel is symbolised with A_{ch}. The diffusion coefficient, D_{ibulk}, is the bulk corrected diffusion and d_h is the hydraulic diameter of channel.

The Sherwood number, Sh, is a dimensionless parameter which is defined as

$$Sh = \frac{h_m d_h}{D_{ij}} \tag{2.66}$$

where h_m is the mass transfer coefficient (moles/(m^2·s)) and D_{ij} is the diffusion coefficient (m^2/s) of the species i in species j.

For the flow channel, the Sherwood number was derived by the analogy between heat and mass transfer. The Nusselt number correlation [32, pg. 3-48] for a three sided adiabatic square duct, with one constant heat flux wall was converted into a Sherwood number by using the following conversion formula [30, pg. 356]

$$Sh = (\frac{Sc}{Pr})^{1/3} Nu \tag{2.67}$$

where Pr is the Prandtl number and the Schmidt number is defined as

$$Sc = \frac{\mu}{\rho D_{ij}} \tag{2.68}$$

With an estimated value of Nu = 2.4 [32, pg. 3-48] for a square channel and standard values [33] for Pr, ρ, and μ the value of the Sherwood number is approximately 2.3.

The concentrations of reactants are calculated using logarithmic averages. A logarithmic average is defined as [33, pg. 291]:

$$C_{\ln} = \frac{\Delta C_1 - \Delta C_2}{\ln\left(\frac{\Delta C_1}{\Delta C_2}\right)} \tag{2.69}$$

where

$\Delta C_1 = C_s - C_{inlet}$ represents the inlet concentration difference and

$\Delta C_2 = C_s - C_{outlet}$ represents the outlet concentration difference.

Using eq. [2.54], the total area of the channel that is exposed to the electrode is

$$A_{ch} = w_c L_{ch} \tag{2.70}$$

The pressure drop in the channel is calculated by eq. 2.71 [26, pg. 333]

$$\Delta p = \rho g h_f \tag{2.71}$$

$$h_f = f \frac{L V^2}{d_h 2g} \tag{2.72}$$

for a square channel in the laminar flow regime,

$$f = \frac{56.91}{Re} \tag{2.73}$$

Substituting into eq. 2.71

$$\Delta p = \frac{56.91 \mu L v}{2 d_h^2} \tag{2.74}$$

where L_{ch} is the length of channel, v is the average velocity in the channel, d_h is the hydraulic diameter of the channel and μ is the average viscosity of gas mixture. Assuming a linear drop in pressure, the average pressure in the cell is

$$p_{av} = p_{inlet} - \frac{1}{2}\Delta p \tag{2.75}$$

2.5.2 Plate Resistance

The value of resistance can be calculated by modelling a cross section as a plate resistor in series with a parallel connection of plate support resistors. Figure 2.4 shows how the cross section of the plate is translated into a resistor network. For this analysis, we assume that the current density is constant, and that the graphite is isotropic with respect to current. To derive the plate resistance, the plate cross section is translated into an equivalent resistor network. The value of the plate resistance is

$$R_p = \frac{\rho h_p}{WL} \tag{2.76}$$

where R_p represents the resistance of the top portion of the plate and ρ is the resistivity of the plate material. W and L are the width and length of plate, and h_p is the distance from the top of the plate to the top of the channel. The resistance in each support is

$$R_s = \frac{\rho h_{ch}}{w_s L} \tag{2.77}$$

where h_{ch} is the height of the channel and w_s is the width of the channel support. The equivalent resistance of the parallel network of support resistors is

$$R_{||} = \frac{R_s}{n_g + 1} \tag{2.78}$$

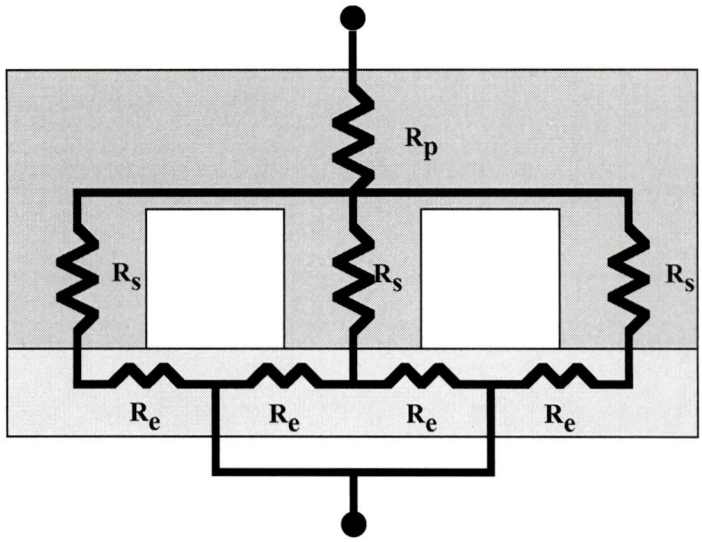

Figure 2.4: Cross sectional representation of resistance in the electrode and plate

If the support widths are the same width, then

$$w_s = \frac{W - n_g w_{ch}}{(n_g + 1)} \tag{2.79}$$

By substituting the equivalent resistance for the channel supports, the resistance can be approximated as

$$R_p = \frac{\rho}{L}\left(\frac{h_p}{W} + \frac{h_{ch}(n+1)}{(W - n_g w_{ch})n_g}\right) \tag{2.80}$$

Table 2.5 shows the base values used for the various parameters. Channel dimensions were based on dimensions from a Ballard Mark V plate.

2.6 Individual Gas Properties

Assuming ideal gas properties for each individual gas component, it is possible to estimate the diffusion coefficient, and the partial pressures and mole fractions.

Parameter	fuel channel (H_2)	oxidant channel (air)
length (mm)	50	50
width (mm)	50	50
thickness (mm)	4.0	4.0
resisitivity (Ωm)	60×10^{-6}	60×10^{-6}
channel cross section	square	square
height (mm)	2.0	2.0
width (mm)	2.0	2.0
number of grooves	12	12

Table 2.5: Plate Properties

Gas	T_c (K)	P_c (atm)
H_2	33.2	12.8
N_2	126.0	33.5
O_2	154.6	50.1
H_2O	647.2	218.3

Table 2.6: Table of Critical Gas Properties

2.6.1 Diffusion Coefficients

The Slattery-Bird approximation [8] was used to estimate the binary diffusion coefficients in the gas mixtures. This correlation is of the form

$$PD_{ij} = a\left(\frac{T}{\sqrt{T_{ci}T_{cj}}}\right)^{b}(p_{ci}p_{cj})^{1/3}(T_{ci}T_{cj})^{5/12}\left(\frac{1}{M_i}+\frac{1}{M_j}\right)^{1/2} \tag{2.81}$$

where PD_{ij} is the pressure diffusivity product constant ($atm\ cm^2/s$), T_{ci} is the critical temperature of species i (K), p_{ci} is the critical pressure of species i (atm), and M_i is the mass of one mole of species i (g). Table 2.6 gives the values [34, pg. 652] for critical temperature and pressure.

System	Temp (K)	PD_{AB} (obs)	Slattery Bird	% error
$H_2 - H_2O_{(g)}$	307	0.915*	1.27	38.8
$O_2 - N_2$	298	0.22**	0.210	4.5
$O_2 - H_2O_{(g)}$	352	0.352*	0.375	6.5

Table 2.7: Comparison of Slattery Bird approximations and experimental values

* - taken from [25, pg. 559]
** - taken from [35]

These values give reasonable approximations for PD_{ij}. A comparison is given in Table 2.7.

Although the value of PD_{ij} for $H_2 - H_2O_{(g)}$ is off by almost 40%, it should not significantly affect the model performance because it is known that the mass transport limitations occur in the cathode catalyst layer. A more accurate approximation should be considered if a detailed analysis of the H_2 sideis to be done.

2.6.2 Water Vapour Pressure

To estimate the saturation pressure of water vapour in the mixture, the following empirical relation [15, pg. 2336] is used.

$$\log_{10} P_{sat} = -2.1794 + 0.02953T - 9.1837 \times T^2 + 1.4454 \times T^3 \tag{2.82}$$

where P_{sat} is in atm and T is in Kelvin units.

2.6.3 Ideal Gas Law

To calculate the concentrations, stoichiometries and pressures, it is assumed that the gas streams follow the ideal gas law. With this assumption,the gas concentration

can be determined using

$$C_i = \frac{p_i}{\bar{R}T} \tag{2.83}$$

where p_i is the partial pressure of the gas species (Pa), $\bar{R}$ is the universal gas constant (J/(mole K)), and T temperature of stream (K).

The outlet concentration is calculated in a similar fashion. However, the molar flow of reactant must be reduced by the amount of reactant consumed by the electrochemical reaction. That is,

$$N_{outlet} = N_{inlet} - \frac{I}{nF} \tag{2.84}$$

2.7 Gas Mixture Properties

The properties of a gas mixture are not the same as each individual gas property. Diffusion coefficients, thermal conductivity, and viscosity are all dependent upon the composition of the mixture. The formulation used to approximate these properties is described below.

2.7.1 Bulk Diffusion

Previous models [8, 14] use the Stephan-Maxwell equation to model diffusion at the cathode. To simplify this more complicated approach, this model uses a bulk diffusion approximation to obtain an approximation for the diffusion of O_2 with respect to the rest of the air mixture. Converting the general formula [31, pg. 637]

$$D_i = \frac{(1 - x_i)}{\sum_{i \neq j} (\frac{x_j}{D_{ij}})} \tag{2.85}$$

to an equation for our $O_2 - N_2$–steam system, we get:

$$D_{o_2} = \frac{(1 - x_{o_2})}{(\frac{x_{N_2}}{D_{o_2-N_2}} + \frac{x_{H_2O}}{D_{o_2-H_2O}})} \tag{2.86}$$

2.7.2 Viscosity

Because the composition of the gases changes within the cell, it is necessary to approximate the properties of the gas mixtures. For each individual species, viscosity is calculated with a Sutherland approximation [26, p. 24].

$$\mu_i = \mu_0 \left(\frac{T}{T_0}\right)^{3/2} \frac{(T_0 + S_0)}{(T + S_0)} \tag{2.87}$$

where S_0 is the Sutherland constant for that particular species, T_0 is the reference temperature, and μ_0 is the viscosity at reference temperature. Values for these properties are easily found in the literature [36].

Once these properties are established, the viscosity of the mixture can be calculated with

$$\mu = \sum_{i=1}^{N} \frac{x_i \mu_i}{\sum_{i=j}^{N} x_j \phi_{ij}} \tag{2.88}$$

where

$$\phi_{ij} = \frac{1}{\sqrt{8}} \left(1 + \frac{W_i}{W_j}\right)^{-1/2} \left[1 + \left(\frac{\mu_i}{\mu_j}\right)^{1/2} \left(\frac{W_j}{W_i}\right)^{1/4}\right]^2 \tag{2.89}$$

and W_i is the molecular weight of the species i, μ_i is the viscosity of the species i, and x_i is the mole fraction of species i. Table 2.8 shows the base values used for gas parameters.

Parameter	fuel (H_2)	oxidant (air)
Temp (K)	350	350
Pressure (atm)	3.0	3.0
Composition	100%H_2	80% N_2/20% O_2
Humidification	100%	100%
Stoichiometry	1.5	3.0

Table 2.8: Base gas parameters used in the present model

Chapter 3

Results and Discussion

A sensitivity analysis was done for various design parameters that were applicable to engineering work. Where data were available, the predictions of the present model were validated against experimental data to determine the accuracy of the model. The sensitivity analysis also highlights areas where cell performance has the potential for improvement. Conversely, if the relatively insensitive parameters are known, they can be substituted with more cost effective alternatives that will not adversely affect performance.

3.1 Overall Model Validation

It is useful to determine the areas that have the largest contribution to performance loss. The polarisation plot in Fig. 3.1 shows the relative contributions to losses from the different processes in the cell. Clearly, oxygen overpotential is the major source of losses for most current densities of practical importance. Membrane losses are the next largest source of losses. These become more significant at higher current

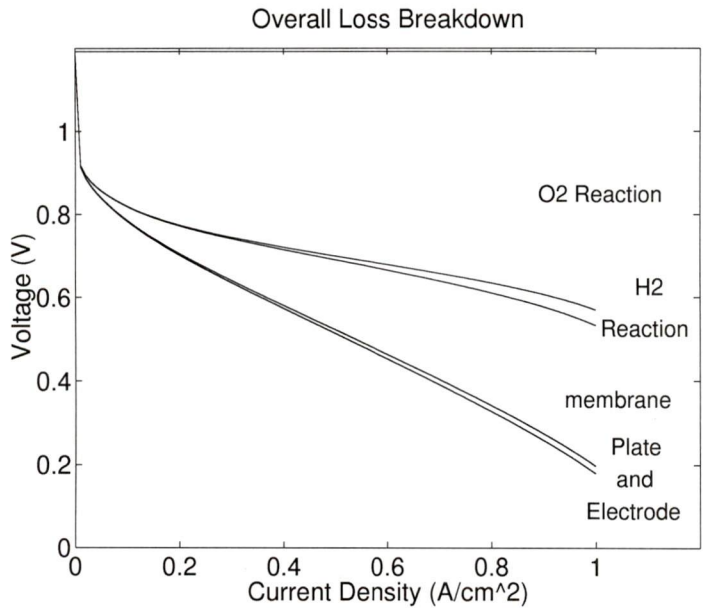

Figure 3.1: Loss contribution for base conditions

densities. Ohmic losses in the electrode and plate are very small by comparison, and comprise less than 5% of the overall losses in the cell. Anodic losses are also very small.

Comparisons with other models' results are encouraging. Bernardi's loss breakdown [14] showed similar results, except that both ohmic and anodic losses were slightly higher. While Springer [15, 16] did not provide a comprehensive breakdown for his models, he ignored ohmic losses and anodic overpotential, stating that they were insignificant compared with other losses. These assumptions are confirmed with the present model.

An empirical model of the Ballard Mark IV cell was developed by Baumert at the Royal Military College in Kingston. This model, referred to as the RMC model, predicts the behaviour of a Ballard Mark IV fuel cell between current densities of 0 to 0.5 A/cm^2, and temperatures between 328 and 358 K [10, pg. 152]. Both the RMC model and this one use the same catalyst loadings and membranes.

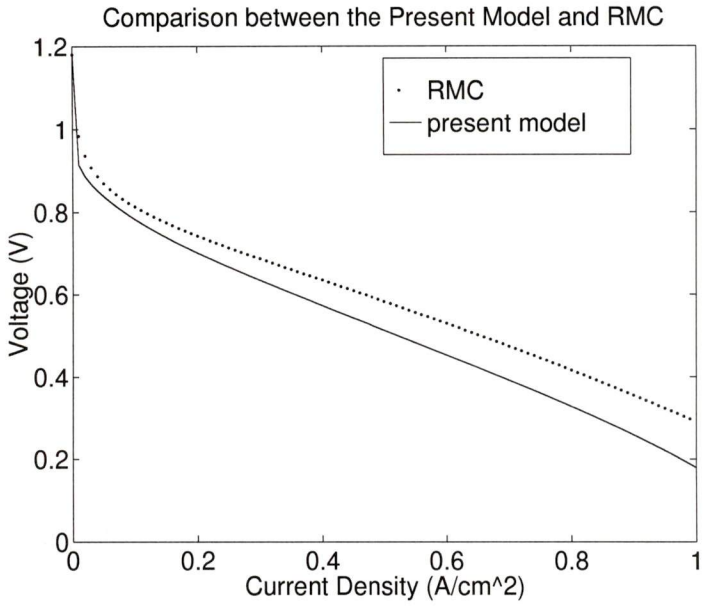

Figure 3.2: Comparison of the present model and the RMC model at base conditions

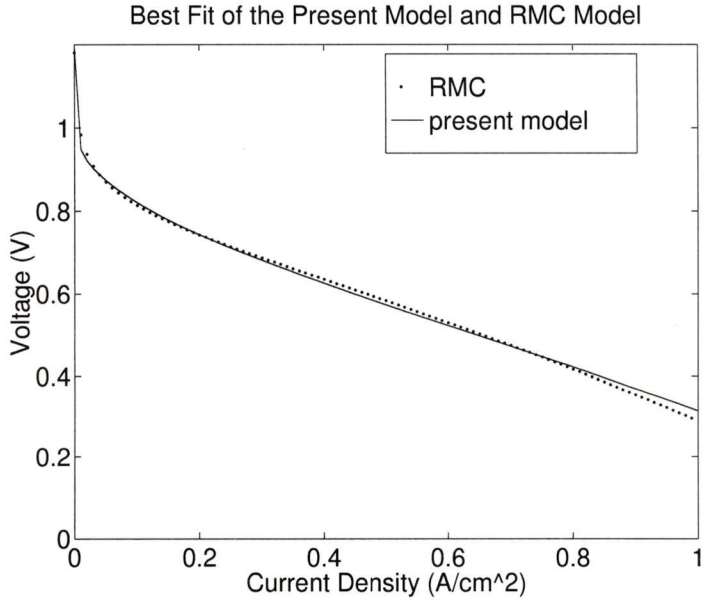

Figure 3.3: Best fit of the present model to the RMC model by increasing exchange current density

Figure 3.2 shows a comparison of the two models for the same base conditions and operating points. As seen in this figure, the present model predicts more conservative performance than that predicted by the RMC model. Figure 3.3 shows that increasing the product of $A_v C_{O2} I_0$ by a factor of three, decreasing membrane thickness from 230 to 210 $\mu\ m$, and increasing void fraction from 40% to 50% gives a model prediction that agrees very well with the RMC model.

3.2 Effect of Design and Operating Parameters

In this section, the effect of design and operating parameters on cell performance is presented. Operating parameters, such as pressure, and design parameters, such as plate resistivity, were changed to see the effect on performance and, where available, compare the predictions with experimental results.

3.2.1 Effect of Temperature

The effect of temperature on cell performance is shown in Fig. 3.4. The present model predicts some sensitivity to temperature variations, and an increase in cell performance as temperature increases. Figures 3.5, 3.6 and 3.7 show the power output, heat production and cell efficiency for the same temperature variations. These curves also have similar responses to temperature. Because these output parameters can be easily derived from the polarisation curve, discussion of the results will hereafter be limited to polarisation curves.

Empirical data from Ballard Power Systems [37] suggests that there is approximately a 30% increase in operating voltage from 300 to 350 K. Experimentally, the magnitude of the voltage change seems much greater than what is predicted by the

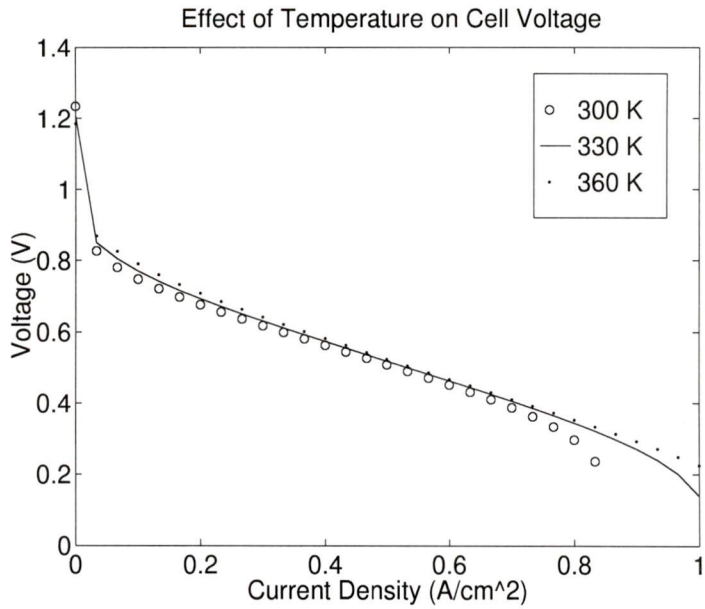

Figure 3.4: Effect of Temperature on cell voltage at base conditions

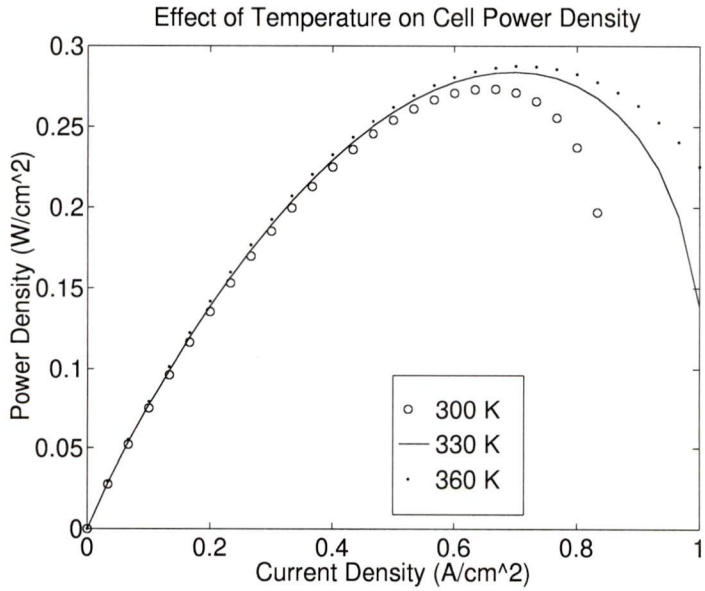

Figure 3.5: Effect of Temperature on cell power at base conditions

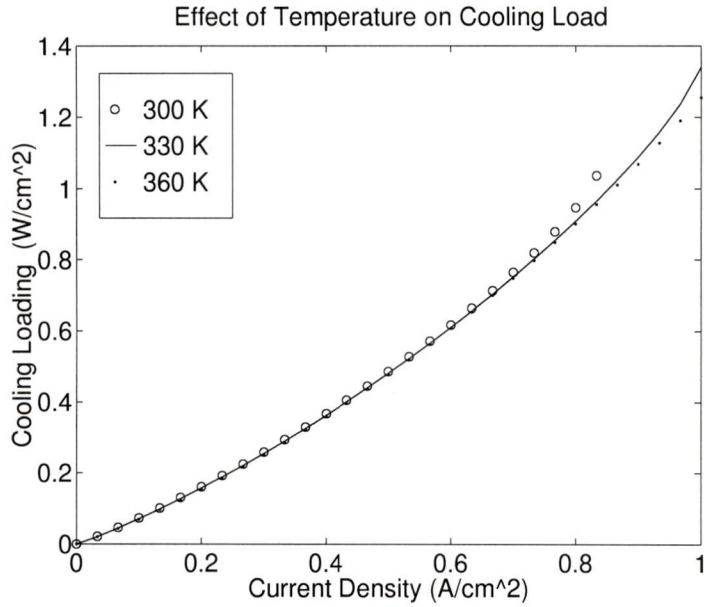

Figure 3.6: Effect of Temperature on cooling load at base conditions

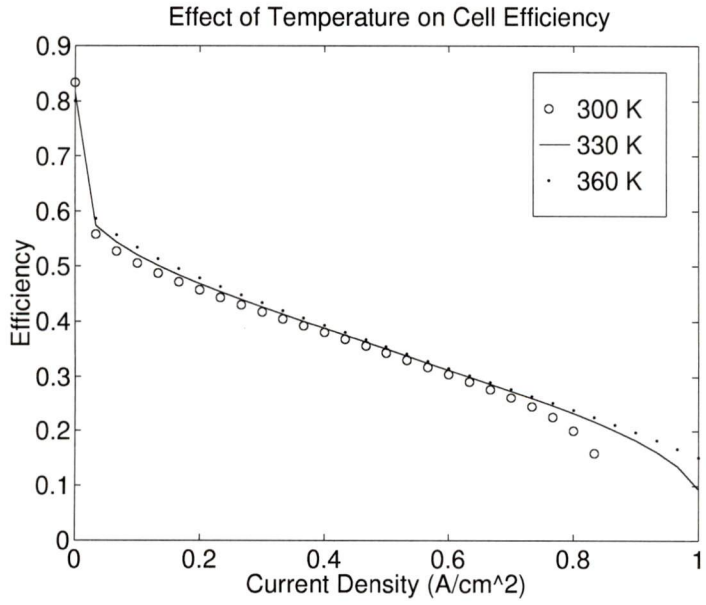

Figure 3.7: Effect of Temperature on cell efficiency at base conditions

the present model. From the Nernst equation (2.2), the open circuit potential will decrease slightly with increasing temperature. This behaviour will help to partially offset any gains in cell voltage from the reduced resistance to electrochemical reaction at higher temperatures.

An investigation into the effect of temperature on electrochemistry indicates some sensitivity to temperature, but not a significant enough sensitivity to match the empirical data. The smaller than expected sensitivity to temperature is due to counteracting factors within the formulation. The formulation for the cell current is given by

$$\frac{dI_z}{dz} = A_v I_{0ref} \left(\frac{C_{o2}}{C_{o2ref}} \right) \left[\exp\left(\frac{\alpha_a F \eta}{RT} \right) - \exp\left(\frac{-\alpha_c F \eta}{RT} \right) \right] \tag{3.1}$$

where I_{0ref} is of the form

$$\log(I_{0ref}) = a - \frac{b}{T} \tag{3.2}$$

and the constants a and b are given in eq. (2.10).

Higher temperatures increase exchange current densities. However, higher temperatures also decrease the open circuit voltages and increase Tafel slopes. For the electrochemistry, any increase in performance from raising temperature is partially compensated for with decreases in other processes.

If the electrochemical model only partially accounts for the discrepancy, then the deviation from experimental data is likely due to two phenomena not accounted for in the present model. First, the model does not account for flooding in the cell. Liquid water condensation is more likely to occur at lower temperatures. Flooding would effectively restrict oxygen diffusion, and lower the overall performance. Second, changes in membrane conductivity will also affect cell performance. Ionic conductivity

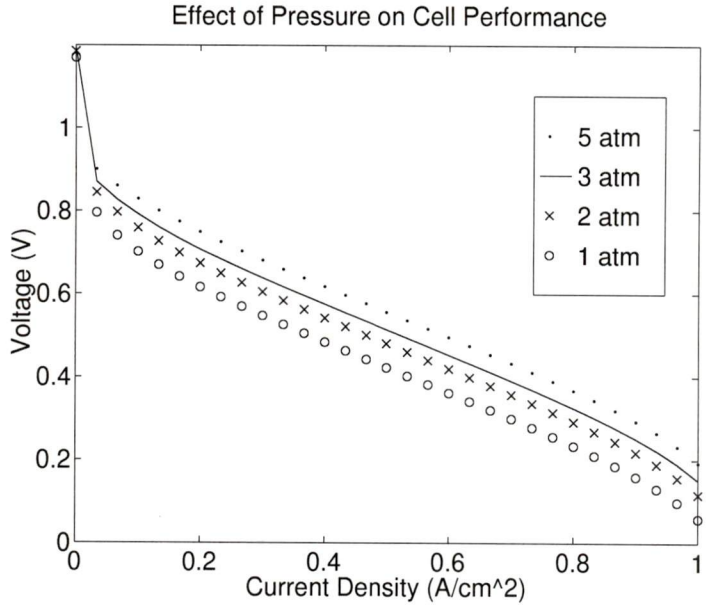

Figure 3.8: Effect of pressure on cell performance for a flooded catalyst layer

in the membrane is dependent upon the water content in the membrane. Increasing temperature past a threshold temperature will cause membrane dehydration, and consequently, lower cell performance.

3.2.2 Effect of Pressure

The effect of pressure on performance for a flooded layer is shown in Fig. 3.8. These results are similar to what has been seen empirically. As a comparison, Fig. 3.9 shows the effect if the catalyst layers are assumed to be unflooded. It can be seen from the two graphs that flooding the catalyst layer makes the cell more sensitive to pressure variations, and lowers the performance at higher current densities. This is due to the difference in diffusion and concentration profiles for gas and liquid phase kinetics. The decreased diffusion coefficient will lower the concentration of reactant, causing an overall lower potential in the cell. In addition, liquid layer will have a

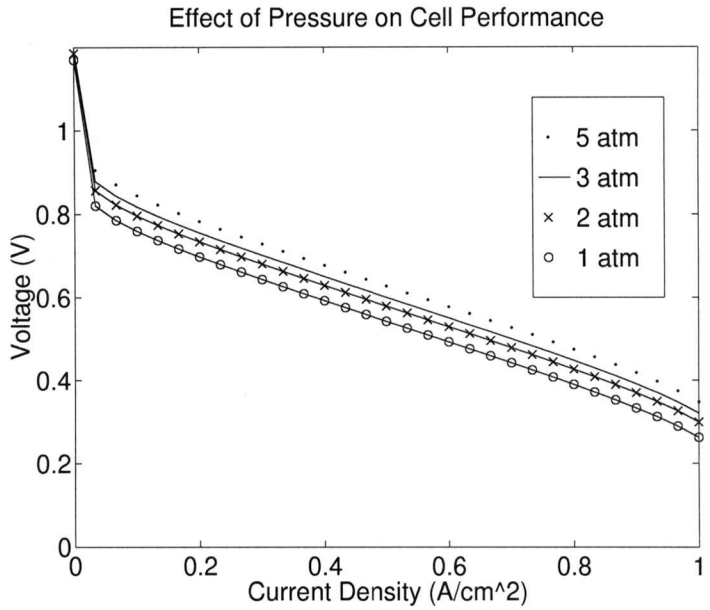

Figure 3.9: Effect of pressure on performance for an unflooded catalyst layer

higher concentration gradient, making it more sensitive to pressure, and therefore concentration, changes at higher current densities.

3.2.3 Effect of Stoichiometry

Figure 3.10 shows the effect of changing the H_2 stoichiometry on the cell performance. This model shows very little change in overall performance. Extremely low stoichiometries show inferior performance, but improvements from increasing stoichiometry level off as the stoichiometry value approaches approximately 1.2. Overall, H_2 stoichiometry does not significantly affect performance. Experimental data from Ballard [38] also indicates that H_2 stoichiometry has very little effect on performance at this pressure.

Figure 3.11 shows the effect of holding the H_2 stoichiometry at 1.5 and varying the O_2 stoichiometry from 1.5 to 5. The plot indicates diminishing returns for

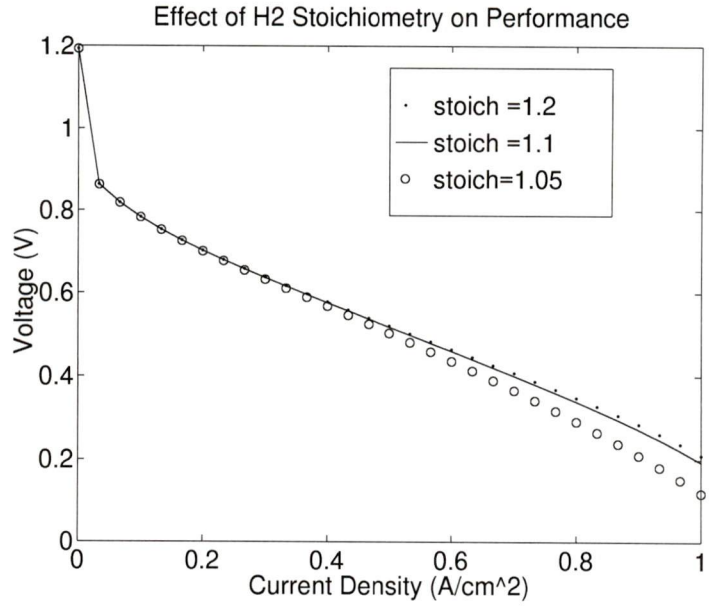

Figure 3.10: Effect of H2 stoichiometry on cell performance

increasing stoichiometry. Overpotential is dependent upon concentration. If the stoichiometry is low, the concentration approaches zero at the outlet of the cell. Because a logarithmic average is used to calculate the O_2 concentration, increasing stoichiometry will increase the concentration of O_2 nonlinearly.

Of interest is the sensitivity of the high current density area to stoichiometry. The probable reason for this sensitivity is the way that the flow channel is modelled. In the present model, there is one channel running through each plate. This channel becomes quickly depleted of oxygen, making its performance very sensitive to the gas flow, and consequently, the stoichiometry.

3.2.4 Effect of Oxygen Concentration

Changing the oxidant gas composition becomes more important for the maximum current density of the cell. As seen in Fig. 3.12, using pure O_2 improves overall cell

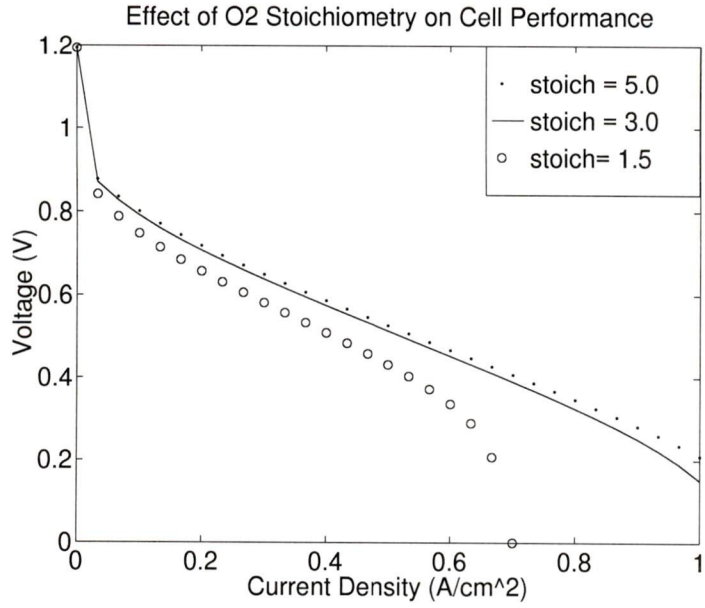

Figure 3.11: Effect of oxidant stoichiometry on cell performance

performance, and reduces the effects of mass transport limitations. The plot shows a gas stoichiometry of 1.5 for both pure and 20% streams, and 3.0 for the 20% stream. It can be seen that the 100% O_2 stream is only marginally affected by changes in this range of stoichiometry, while the air stream shows a much higher sensitivity for the same range. Again, this is due to the overall concentration of O_2. The 100% pure O_2 stream is not depleted for this stoichiometry range. For the case of the 20% stream, the O_2 is depleted much more quickly, lowering the O_2 concentration more quickly, and consequently increasing the amount of overpotential.

3.2.5 Electrode Parameters

Electrode void fraction was changed from 0.2 to 0.6, as seen in Fig. 3.13. Increasing void fraction in the electrode increases mass transfer and simultaneously increases electrode resistance. The corresponding increase in resistivity from increased void

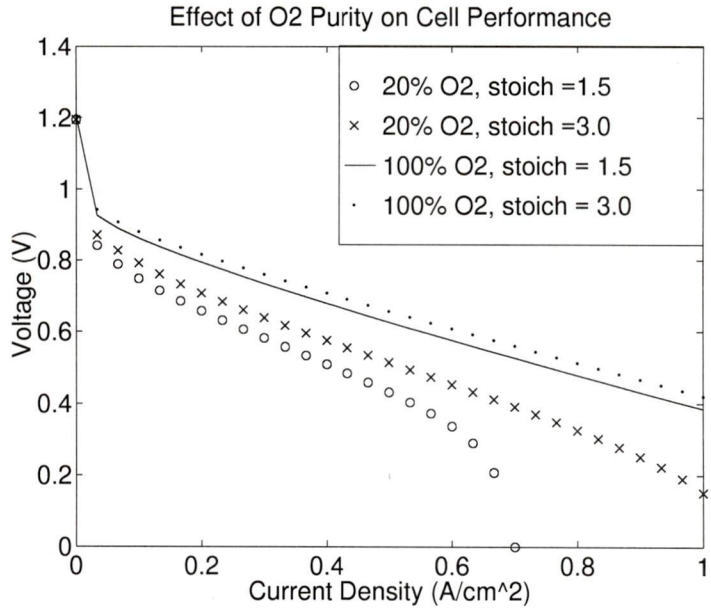

Figure 3.12: Effect of changing oxidant stoichiometry from 1.5 to 3.0 for both air and 100% pure O_2

fraction is swamped by the increased performance from better gas diffusion. This indicates that increasing void fraction will enhance cell performance. However, due to the structural considerations involved with plates under high pressure, the void fraction will more than likely be limited by the amount of compression due to the pressure necessary to seal the cell.

Holding electrode void fraction constant, the thickness of the electrode was also varied. As seen in Fig. 3.14, the performance prediction is very similar to the void fraction plot of Fig. 3.13. This is expected because both void fraction and thickness affect gas diffusion and electrical resistance. Although it is not easy to see on the plot, at low current densities, a thinner electrode shows slightly lower performance than a thicker electrode. Because increasing the thickness also increases the cross sectional area that electrons can flow through, resistance through the electrode decreases. As current density increases, the lowered resistance is small compared to mass transport

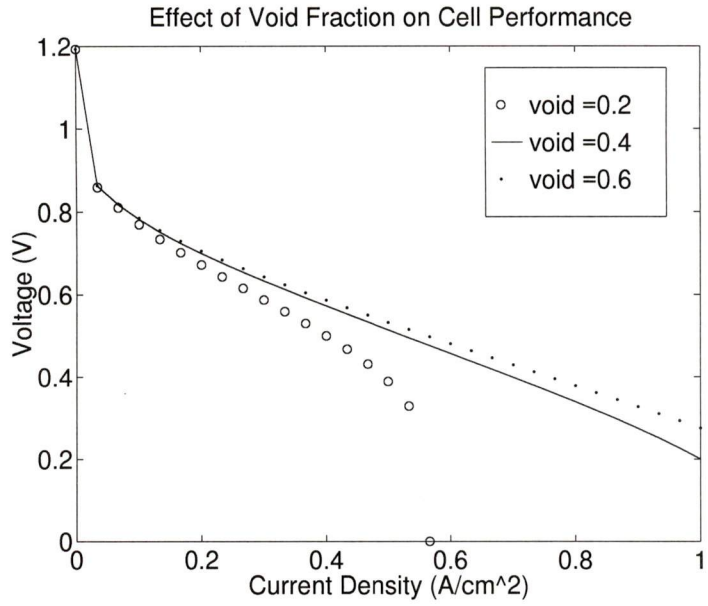

Figure 3.13: Effect of electrode void fraction on cell performance

limitations, causing the overall performance to drop.

The effect of resistivity on cell performance is shown in Fig. 3.15. Increasing the value of the resistivity by two orders of magnitude shows the effect on performance. The upper value of resistivity is roughly the same order as that of conducting polymers. Given this, the electrode material can be made from a conducting polymer, but it is predicted to perform very poorly as current density increases.

3.2.6 Plate Parameters

Plate resistivity and channel configuration were examined in this analysis. Plate thickness was not examined for two reasons. First, as seen earlier, plate losses are very small and changes in thickness are not expected to create large changes in performance. Second, mechanical strength is not accounted for in the present model. It is the fracture point of the plate, and not the ohmic resistance, that will determine

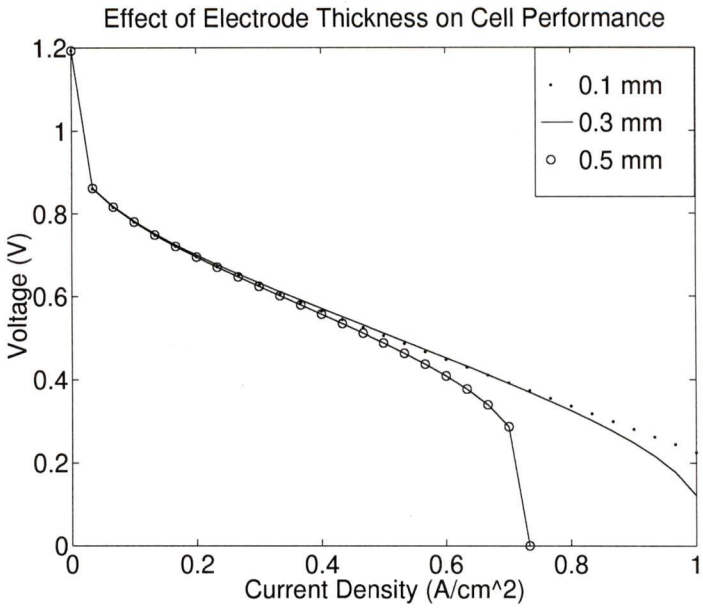

Figure 3.14: Effect of electrode thickness on cell performance

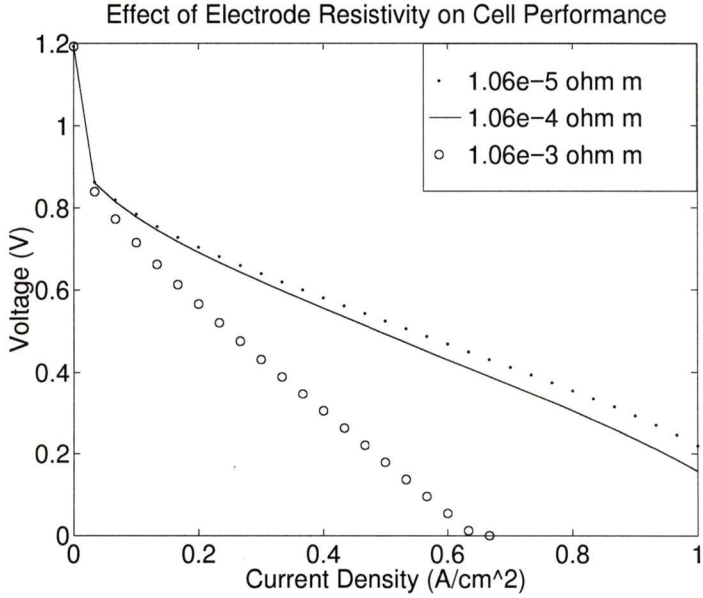

Figure 3.15: Effect of increasing electrode resistivity by two orders of magnitude

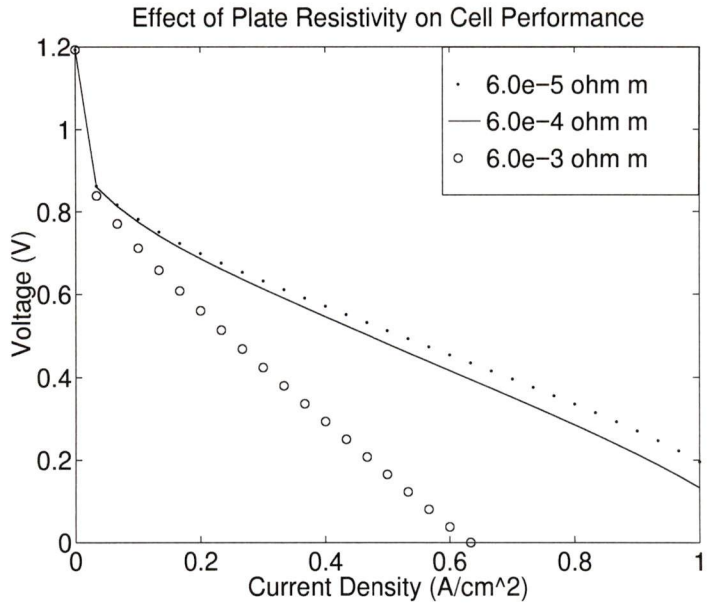

Figure 3.16: Effect of plate resistivity on cell performance

what the minimum plate thickness is. The overall contribution by the plate is small compared with other losses.

Plate resistivity was increased by two orders of magnitude. The performance curves are shown in Fig. 3.16. Like the electrode, the plate could be made with a conducting polymer, but performance would suffer at higher operating points.

Changing the channel configuration may also improve performance. As a first approximation, the present model indicates that increasing the number of channels will increase cell performance. Figure 3.17 shows the effect of changing the number of channels. As seen in the plot, increasing from 6 to 18 channels gives a significant increase in performance. This plot indicates that the amount of surface area exposed to the channel influences where the cutoff current occurs. There are marginal decreases in performance due to increasing resistivity, but overall, if higher current densities are desired, then more surface area in the cell is needed. However, increasing channel area will reduce support area. Reducing the support area will change the void fraction

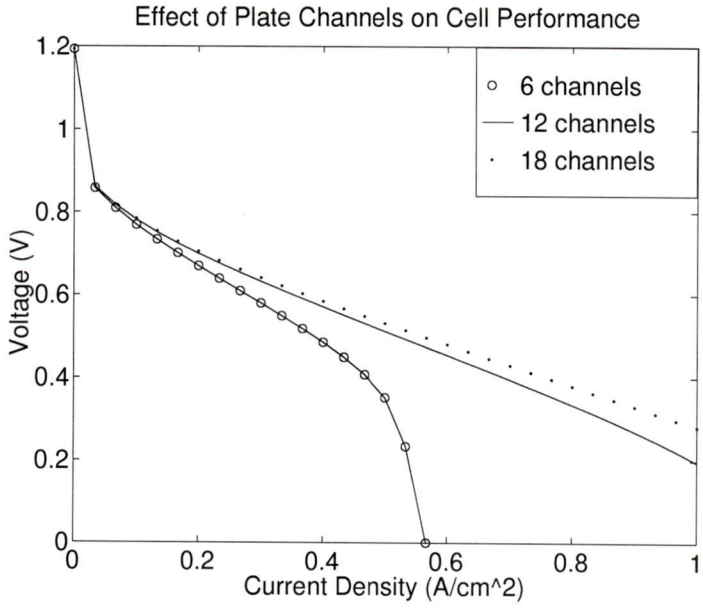

Figure 3.17: Effect of changing the number of channels in the cell

of the electrode because of the increased compression, and consequently change the ability of reactant to diffuse to the catalyst surface directly underneath the support.

3.2.7 Membrane Parameters

The membrane model is based on the work of Bernardi and Verbrugge [13, 14]. One question that has been raised is the value for the hydraulic permeability. According to Bernardi, this value varies by up to two orders of magnitude. To investigate the sensitivity of this variance, the hydraulic permeability in the present model was increased and decreased by two orders of magnitude. No appreciable difference was seen in the polarisation plot, which indicates that this value is not significant for overall performance.

A comparison of the cell performance with Nafion and Dow membranes is shown in Fig. 3.18. This plot shows reasonable qualitative agreement between the

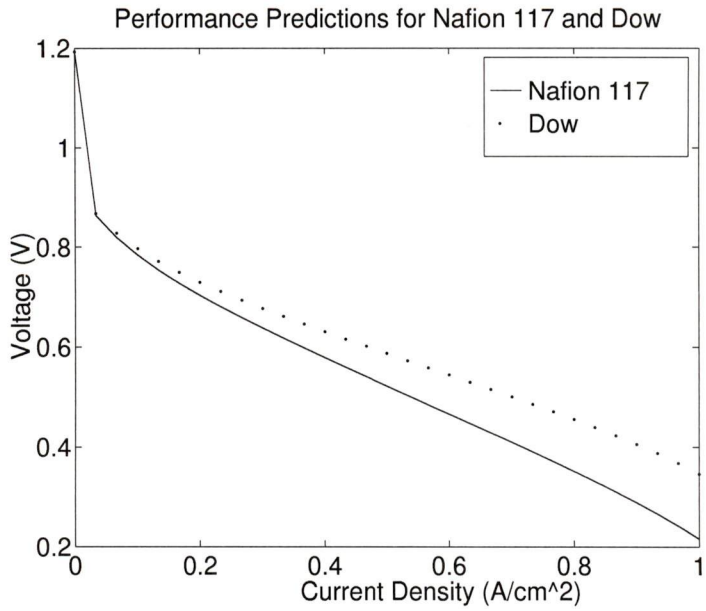

Figure 3.18: Model predictions of performance for Nafion and Dow membranes

performance of the two membranes when compared with other researcher's results. The effect of membrane thickness was examined for a Nafion membrane. Thickness was calculated by assuming a 30% swelling of the dry membrane. Figure 3.19 shows the predicted performance for Nafion 112 (66 μm), 115 (165 μm)and 117 (230 μm). The plot shows the linear increase in performance for decreasing membrane thickness. However, the minimum thickness can not be determined by the present model, because manufacturing difficulties arise as membrane thickness decreases.

Conductivity was changed by increasing the charge concentration parameter in eq. (2.42). The predictions for increasing concentration by 50% and 100% are shown in Fig. 3.20. This plot indicates an inverse relationship for conductivity and performance. consequently, performance decreases linearly with increased membrane resistance.

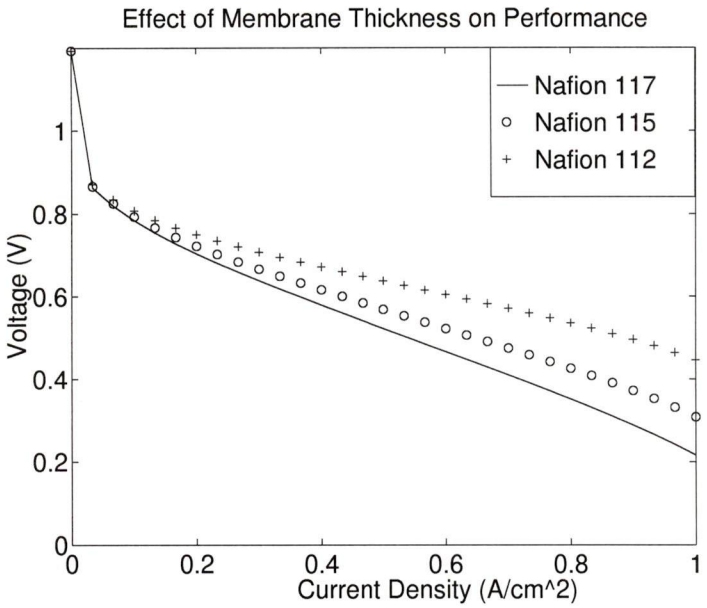

Figure 3.19: Effect of Nafion thickness on cell performance

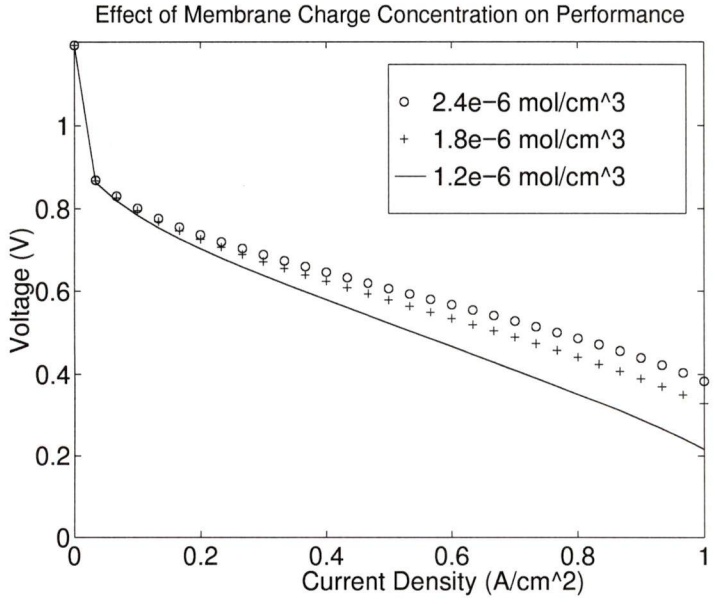

Figure 3.20: Effect of ion concentration on cell performance

3.2.8 Summary

Overall, performance of the catalyst layer and membrane limits the maximum performance of cell. The gas properties and cell configuration have a more significant effect on the maximum operating current densities than on the overall performance of the cell. In other words, to increase the overall efficiency of the cell, the membrane and catalyst layer would be the best areas to concentrate on. To increase the maximum power point, the gas properties and physical construction of the cell would be the areas with the most significant impact.

In the electrode, gas diffusion has a much stronger influence on performance than ohmic resistance. The gas diffusion is influenced by the void fraction, and thickness of the electrode material. Because performance is predicted to be more greatly influenced by gas diffusion than resistivity, it may be possible to substitute higher resistivity materials that have better transport or cost properties, without appreciably affecting the performance of the cell.

Cell performance is more strongly influenced by mass transport parameters than by ohmic resistance. Increasing mass transport by increasing the ratio of channel area to support area will likely increase performance. However, increasing this ratio will also increase the amount of compression in the electrode below the supports. This will affect diffusion in the electrode, and subsequently, performance.

There are two areas in the present model that could significantly improve the predictive abilities. First, development of a two phase water transport model will account for mass transport limitations in the electrode and catalyst layer. Finally, development of a membrane model that can account for drying due to temperature or diffusion effects will remove the linear relationship between current density and resistance and enable the model to better predict performance at higher current den-

sities.

3.3 Effect of Catalyst Layer on Cell Performance

In this section, basic assumptions about the catalyst layer composition and electrochemistry will be investigated to see their effect on the overall performance of the model. The composition of the layer will greatly affect the performance of the cell. Currently, exact knowledge on the composition of the layer and its thickness are not available. However, it is interesting to observe what the predicted effect of changing the composition will have on the overall performance of the cell. For this section, only changes in the cathode side will be discussed. As shown earlier in Fig. 3.1, anodic overpotential is fairly minor, and will not be discussed.

3.3.1 Surface Area

One of the major assumptions of the catalyst layer model is that 100% of the catalyst surface area is active. This assumption may not be true if PTFE coverage or dense packing of catalyst is taken into account. The effect of reducing the active area is shown in Fig. 3.21 for 20%, 60% and 100% of the ideal surface area. Because of the logarithmic dependency on surface area, the output voltage is relatively insensitive to small departures from the ideal surface area. This plot indicates that the 100% assumption will have a small overall effect on the cell performance if the actual coverage does not significantly deviate from literature values.

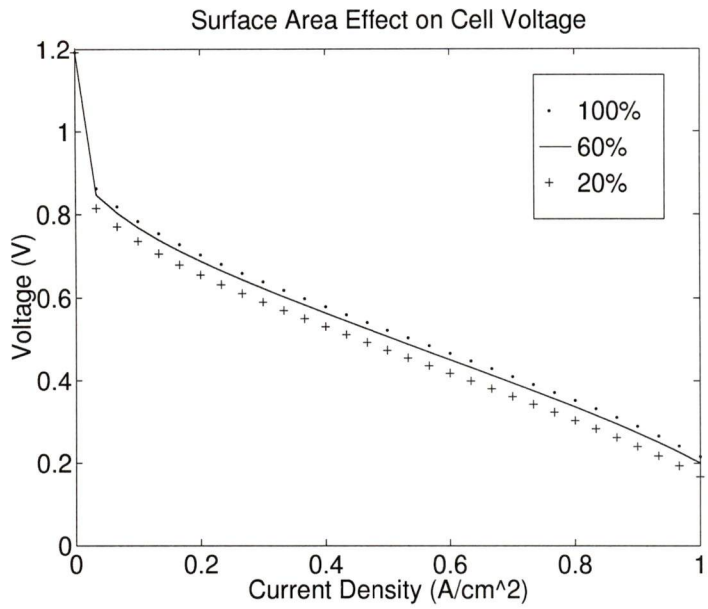

Figure 3.21: Effect of active surface area on cell performance

3.3.2 Void Space Composition

The void space composition was changed to study its effect on the distribution of current and O_2 in the cathode catalyst layer. Figures 3.22 and 3.23 show the changes in current density distribution and O_2 concentration distribution for a water flooded and unflooded void space at a current density of 1.0 A/cm^2. For an unflooded layer, distributions are almost linear. Because of the decreased diffusion coefficient for the gas-liquid case, concentration gradient must increase. For a flooded, 5 μm thick layer, most of the current is produced in the first 20% of the layer. These predictions confirm Bernardi's statement [14] that most of the reaction occurs in the first few micrometers of the layer.

Figure 3.24 shows how the current distribution changes with changing current density. Three current densities of 0.1, 0.5 and 1.0 A/cm^2 are shown. The 0.1 A/cm^2 curve shows that at that current density, mass transport does not seem to be

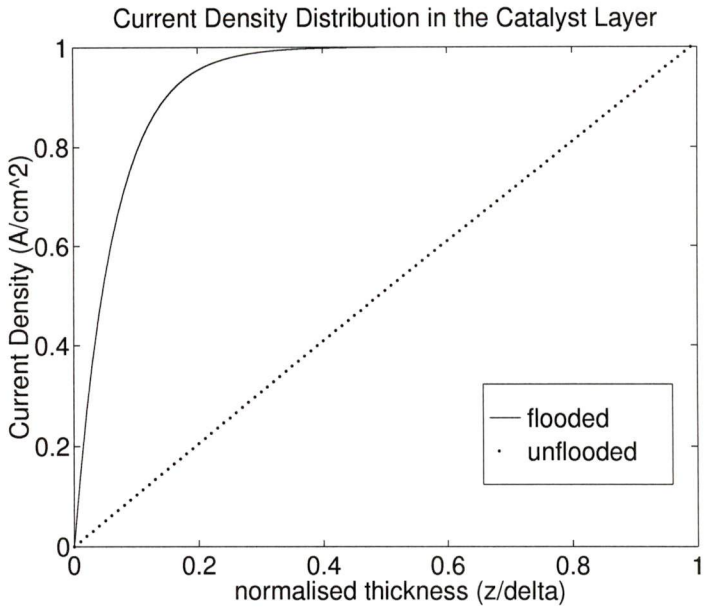

Figure 3.22: Current density distributions for flooded and unflooded void space at 1.0 A/cm^2

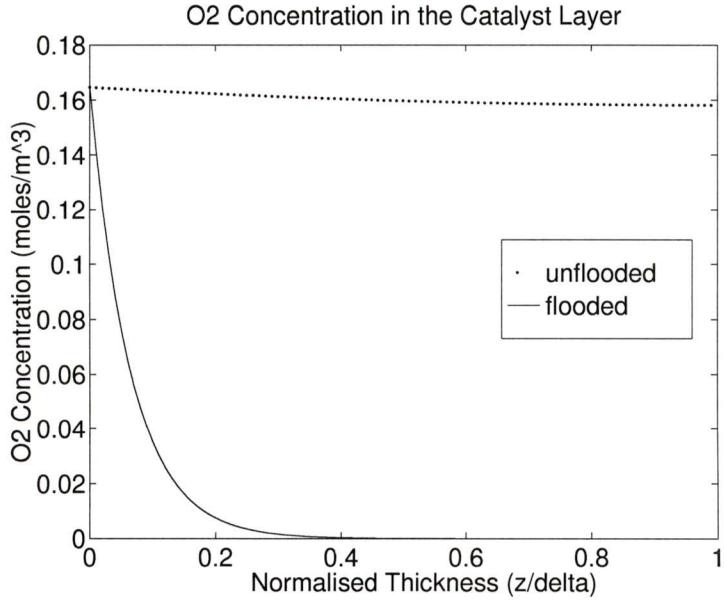

Figure 3.23: O_2 concentration distributions for flooded and unflooded void space at 1.0 A/cm^2

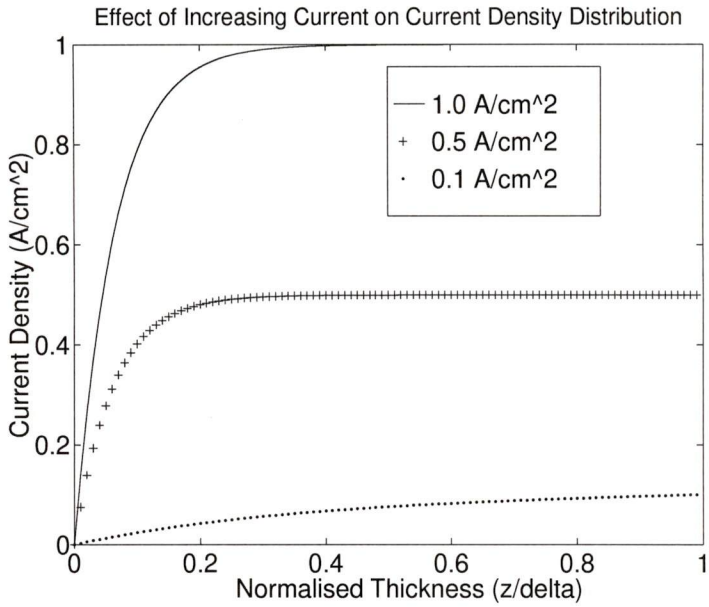

Figure 3.24: Current density distributions for different current densities

significantly affecting the solution. As current density increases, the mass transport limitations become more important, and the majority of the current production shifts towards the electrode side of the catalyst layer.

Figure 3.25 shows the oxygen concentration distributions for the same current densities. Initial values for O_2 concentrations are different because the logarithmic average used to estimate surface concentration of O_2 is dependent upon the current density in the cell. This figure shows how the current density can influence the distribution of O_2 in the catalyst layer.

3.3.3 Flooding

With a slight modification to the catalyst layer formulation, it is possible to make a simple model for flooding in the cell. A liquid film of thickness δ_w is assumed to be on top of the catalyst layer. This thickness is assumed to vary linearly with the current

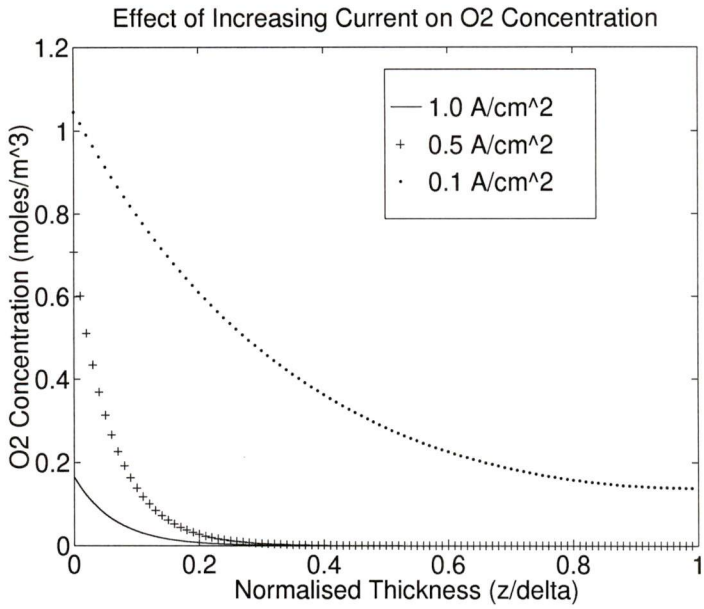

Figure 3.25: Oxygen concentration distributions for different current densities

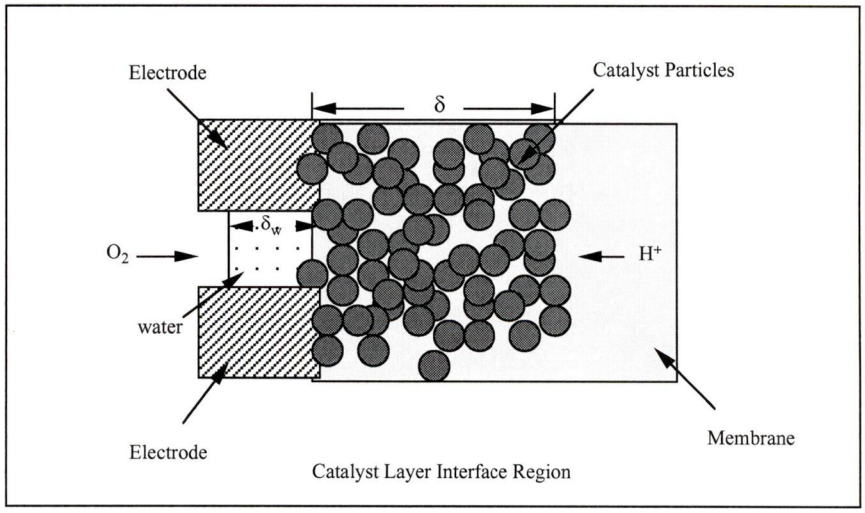

Figure 3.26: Flooded catalyst layer with extra liquid film

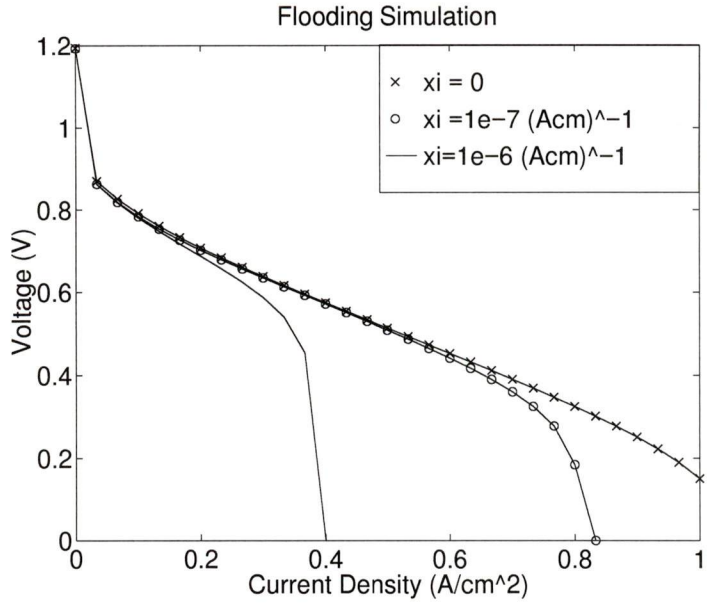

Figure 3.27: Simulation of flooding in the fuel cell

density. Figure 3.26 shows how δ_w has been defined in the catalyst layer model.

$$\delta_w = \xi I \tag{3.3}$$

where ξ is a proportionality constant, δ_w is the thickness of liquid water layer, and I is the current density of the cell.

The results for different values of ξ are shown in Fig. 3.27. Although the exact thickness of the water layer is not known for a flooded cell, qualitatively, this model shows lowering of the maximum current operating point for increasing water thickness. The line for $\xi = 1 \cdot 10^{-8}$ $(\mathrm{A} \cdot cm)^{-1}$ cuts off at approximately 0.4 $\mathrm{A/cm^2}$, indicating that an excess water layer of thickness 0.4 μm will cause a flooding condition. While there is no data yet to quantify the effect, it appears that this model is a reasonable simulation for flooding in the cell.

Chapter 4

Optimisation of the Cathode Catalyst Layer

4.1 Optimum Platinum Loading

Platinum usage is a critical issue in fuel cells. For PEMFCs to be economically feasible, the cost must be in the same range as that of an internal combustion engine. Assuming a Pt load of 4 mg/cm^2, and \$20 CDN/gram of Pt, the approximate Pt cost of a 25 kW fuel cell stack at 430 g/stack is \$8600 CDN, or about \$350 CDN/kW. Given that a typical internal combustion engine costs between \$75 and \$135 CDN/kW, the price of Pt cannot realistically be expected to fall sufficiently to have the price of the stack in a competitive range. Clearly, a reduction of platinum loading is needed if fuel cells are to compete economically with internal combustion engines.

Investigating the use of Pt in the catalyst layer may lead to improvements in performance or reductions in the amount of catalyst. There are two types of optimisation that will be discussed in this section. The first type of optimisation is

the effective use of platinum. In this case, the cell is optimised to make the most effective use of the Pt. The second is performance optimisation. For this case, the point where optimum performance for a particular platinum load is discussed.

4.2 Effective Platinum Use

This section discusses the catalyst layer mass transport in more detail. By investigating the catalyst layer transport more closely, it is possible to determine how effectively the Pt is used for the electrochemical reaction, and how operating conditions can change the effective usage.

Weisbrod [18] analysed optimisation of platinum for performance but did not discuss how well the Pt was being used within the catalyst layer. Bernardi [13, 14] predicted that the majority of the electrochemical reaction occurred in the first μm, and confirmed this with comparisons to the literature. This indicates that Pt is not being effectively used in the catalyst layer.

Because the performance of the cell is determined by the transport of reactants in the catalyst layer as well as the amount of Pt in the layer, mass transport to the catalyst is as important to performance as the amount of catalyst in the layer. Using the catalyst layer model described earlier, reactant concentration and current density distributions in the catalyst layer can be investigated. Examples of these distributions are shown in fig. 4.1 and fig. 4.2.

As seen in fig. 4.2, the O_2 decreases quickly at first, and levels off near the end of the catalyst layer. Current production falls off as well. The point where the concentration of O_2 is almost zero (the ratio of $C_\delta/C_0 < 1\times10^{-9}$) marks the boundary between used and unused Pt. Beyond this point, Pt is no longer being used because there is no O_2 available. Figure 4.3 shows how the zero concentration boundary varies

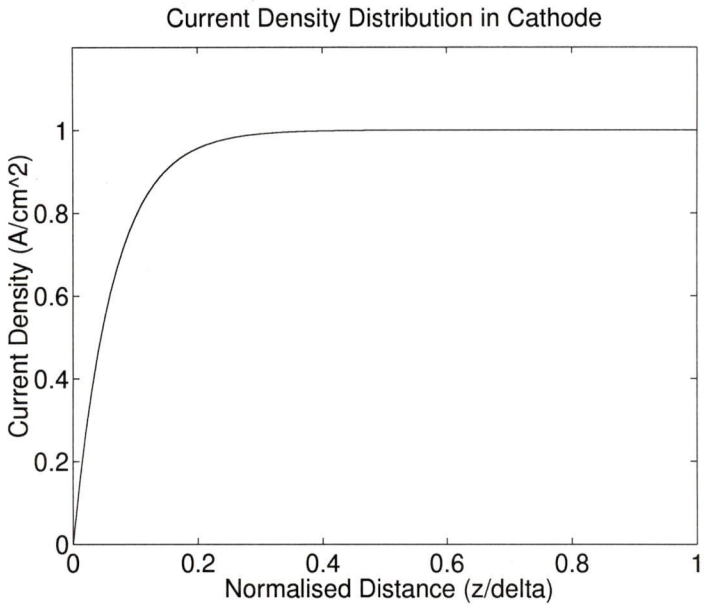

Figure 4.1: Current density distribution in the catalyst layer

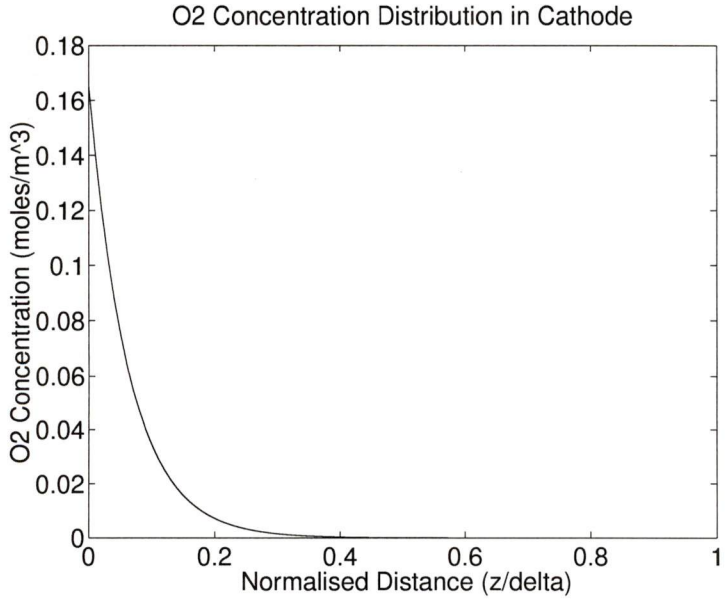

Figure 4.2: Oxygen concentration distribution in the catalyst layer

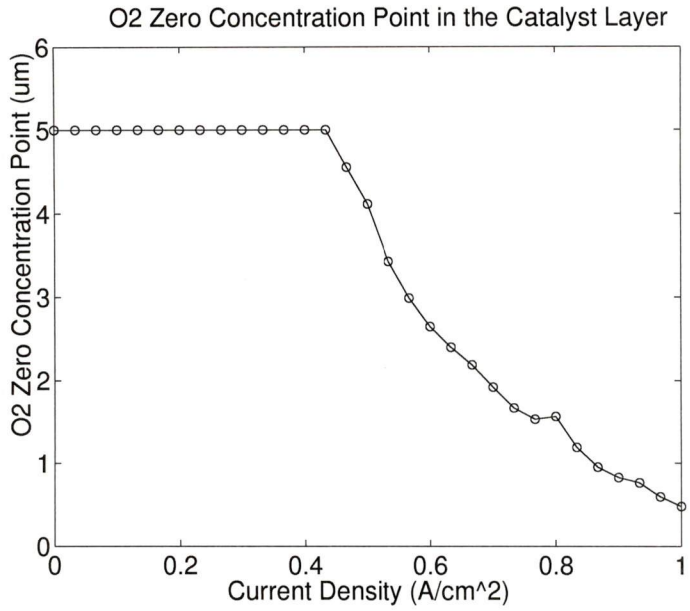

Figure 4.3: Zero O_2 concentration point as a function of current density

with changing current density. As the current increases, the boundary moves closer to the electrode, and consequently, the amount of platinum that is used decreases.

What is indicated with a curve of this nature is that Pt is not used effectively as current density increases. Increasing current density, or output power, allows one to decrease the Pt loading. Figure 4.4 compares the performance of a normal 4 $mg/cm^2, 5\mu m$ thick layer with one where both load and thickness have been reduced to 10% of the original values. The plot shows that performance is inferior at low current densities, but there is no change at high current densities.

Assuming a homogeneous mix of Pt in the catalyst layer, this zero point can be normalised by dividing by the thickness of the layer. This gives a dimensionless parameter which will be referred to as effective Pt use, or ψ_{Pt}. This parameter is a measure of how well reactants are diffusing to the Pt.

To determine the sensitivity of ψ_{Pt} to void fraction and loading, a plot of void

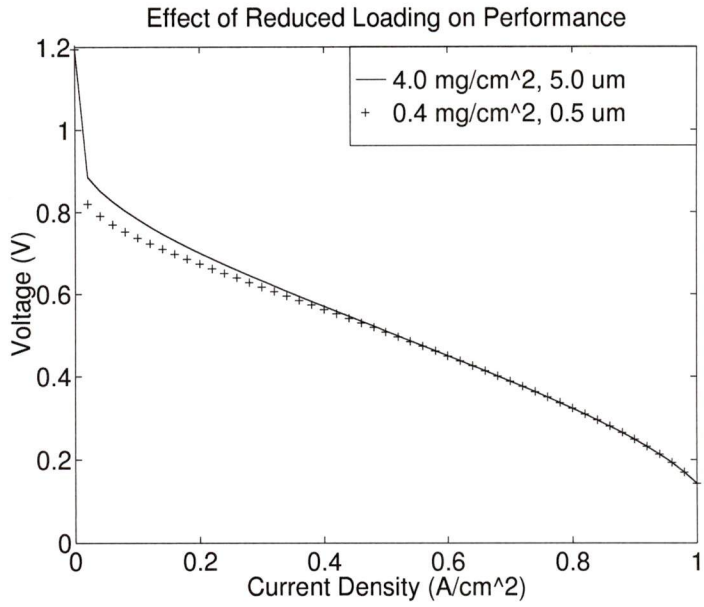

Figure 4.4: Effect on cell performance of reducing both Pt loading and catalyst layer thickness by a factor of ten.

fraction, loading and the resulting overpotential was made for a constant current density of 0.500 A/cm^2. This is shown in Fig. 4.5. As seen from this figure, a void fraction ranging from approximately 0.5-0.7 gives the most effective use of Pt. Fig. 4.6 shows how increasing the current density changes the ψ_{Pt}. The lower plot shows the effective use for a current density of 900 mA/cm^2. Increasing current density lowers the effective Pt use, and decreases the impact of optimal void fraction. At lower loadings, the effective use is much higher because diffusion is easier in a low load (and therefore thinner) layer. At higher loadings, the effective use decreases and the impact of an optimum void fraction is lessened because there is very little Pt being used. This indicates that void fraction is less important than decreased loading at higher current densities.

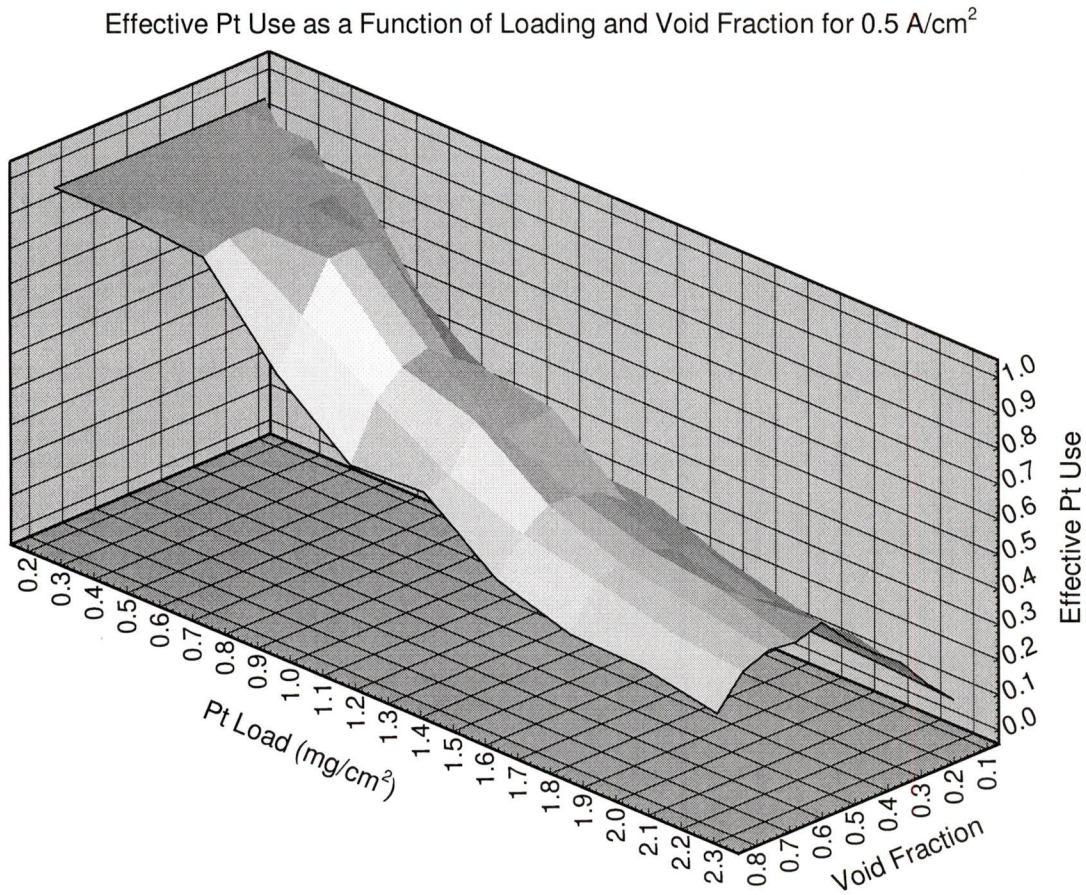

Figure 4.5: Effect of Pt loading and void fraction on the effective Pt use for a current density of 0.5 A/cm^2

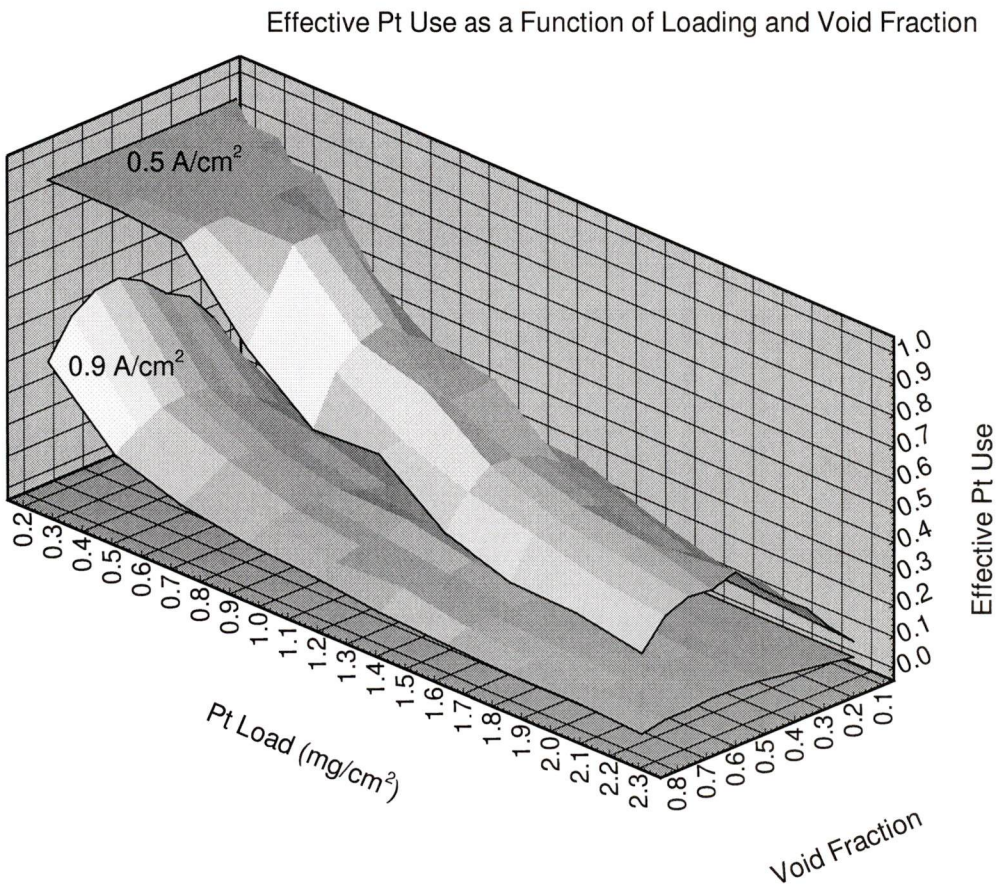

Figure 4.6: Effect of Pt loading and void fraction on the effective Pt use for current densities of 0.5 and 0.9 A/cm^2

4.3 Performance Optimisation

Weisbrod's model showed the existence of [18] an optimal loading of Pt for a given thickness of catalyst layer. This performance optimum for Pt loading occurs because of the tradeoff between increased active catalyst surface area and decreased rate of reactant diffusion.

This model also shows the existence of an optimal load thickness. Although the optimal point occurs at approximately the same loading as that predicted by Weisbrod, the change in voltage for different layer thicknesses is much less. This may be the result of membrane transport factors, which are not implemented in this model.

Figure 4.7 shows the relationship between current density and O_2 overpotential for four different polarisation plots of varying levels of catalyst loading but constant layer thickness. A denser packing of platinum has a higher amount of active surface area, but is more susceptible to mass transport limitations. At high current densities, the densely packed layer has a lower performance than the more loosely packed layers. At low current densities, the curve for 0.3 mg/cm^2 has lower voltage losses than the 0.2 mg/cm^2, but higher overpotential at higher current densities. It can be seen from the curves that there is an optimum value for void fraction that will give the lowest overpotential.

This is better illustrated in Fig. 4.8. This figure shows how O_2 overpotential changes with Pt loading for a constant thickness of catalyst layer. As loading increases, the active surface area is increased and, as a result, overpotential decreases. However, increasing surface area increases the solid volume of catalyst. This decreases the ability of reactant to diffuse through the layer, and lowers the concentration of reactant at the catalyst surface. Lowering reactant concentration will increase the

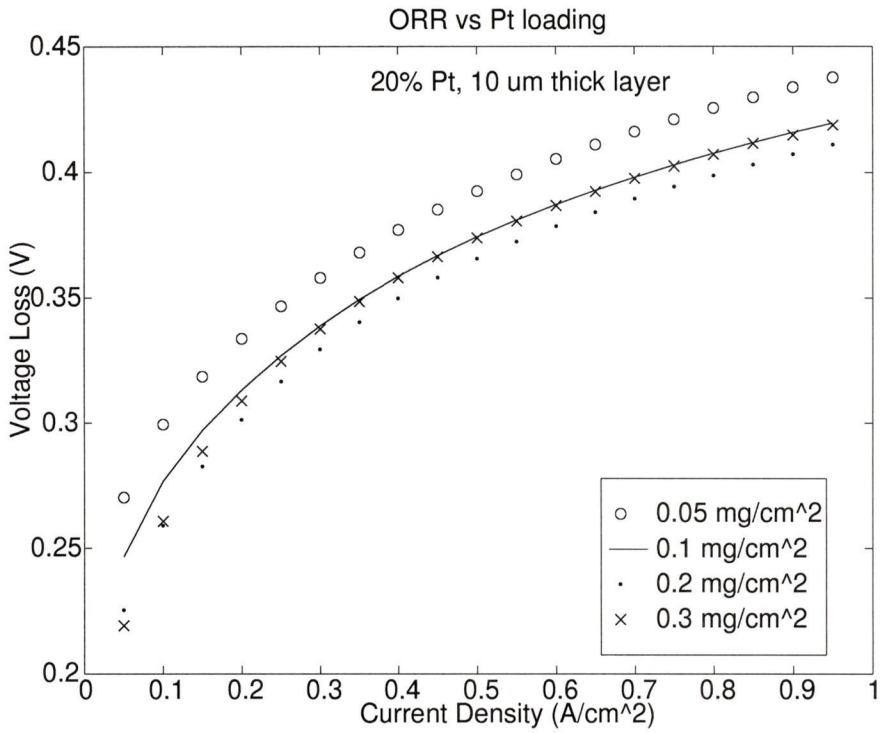

Figure 4.7: Effect of changing Pt load on cathode overpotential for a constant catalyst layer thickness with 20% supported Pt as catalyst

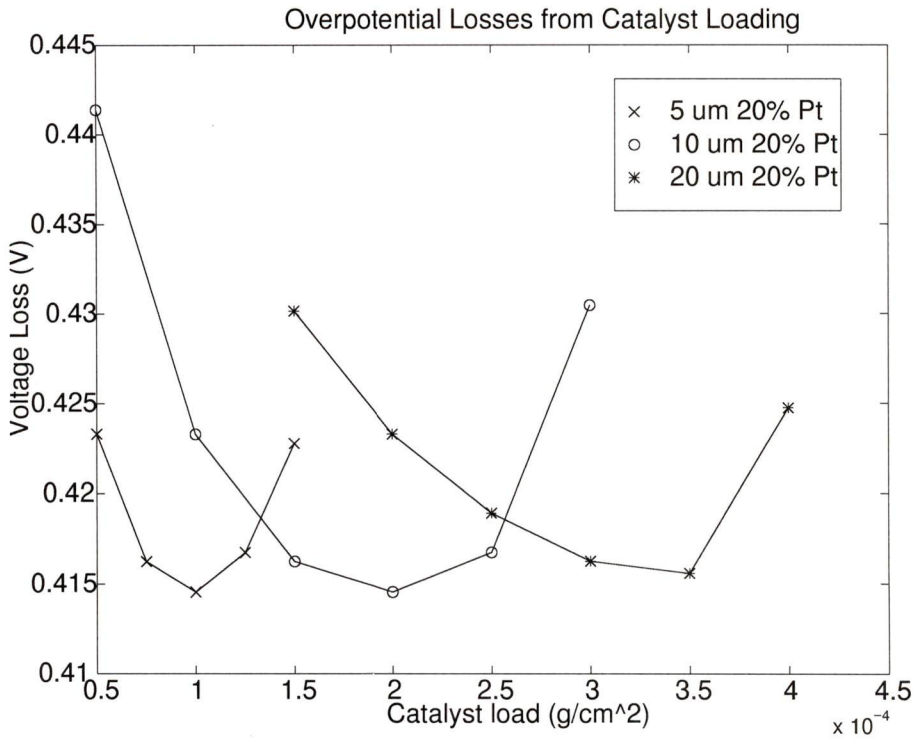

Figure 4.8: Overpotential curves for different catalyst thicknesses

overpotential. Thus, as loading increases, overpotential decreases. However, the gain in performance eventually is overtaken by mass transport limitations. The tradeoff between increasing void fraction and decreasing active surface area determines the location of the lowest voltage losses.

The optimal loading point may change with both catalyst layer thickness and Pt loading. To investigate the effect of changing these parameters, a three dimensional plot of thickness, catalyst loading and cathodic overpotential is shown in fig. 4.9. This is for a current density of 0.5 A/cm^2. As seen in the plot, there are two effects. First, as thickness increases, the parabolic shape of the overpotential vs load line begins to flatten out. Second, as loading increases, the parabolic shape for overpotential and thickness steepens. The region in the far right rises very quickly. This is due to mass

transport effects constricting the supply of oxygen. As the thickness is increased for a fixed Pt load, the ability of oxygen to diffuse increases due to higher void fraction, raising the concentration of oxygen, and therefore lowering the cathodic overpotential. As the layer thickens, the oxygen must diffuse farther, lowering the concentration, and therefore, raising the overpotential.

Holding the thickness constant, increasing the Pt loading lowers the overpotential by providing more surface area for the reaction to occur. However, increasing the Pt decreases the volume the oxygen can diffuse through. Eventually, mass transport difficulties outweigh contributions from Pt surface area, and the overpotential increases despite the increased amount of surface area available for the reaction.

Thus, the optimum loading point is formed by two valleys, which flatten as loadings are lowered and thicknesses are increased. The intersection of these valleys forms a minimum load valley with a gradually increasing thickness and Pt loading. This indicates that there is an optimum void fraction (based on the diffusion coefficient of O_2 in water) that can be exploited for the design and manufacturing of fuel cells with better performance.

4.3.1 Current Density and Optimal Loading

The effect of current density on the optimal loading point was investigated. If the optimal point changes significantly with current density, this would indicate the possibility of enhanced performance at a single operating point. This model predicts that the effect of current density on overpotential will be minimal. Three different current densities were plotted together to observe the relationship between current density and optimal loading. As seen in Fig. 4.10, increasing current density does not have much effect on overpotential. This plot shows three overpotential surfaces

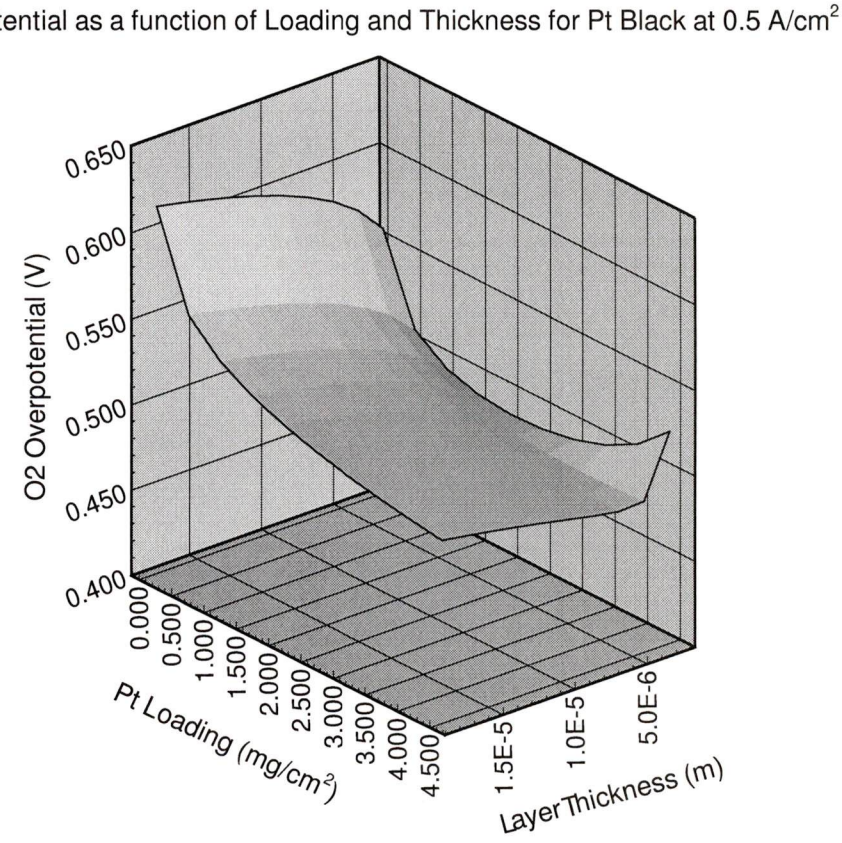

Figure 4.9: Cathodic overpotential as a function of layer thickness and loading

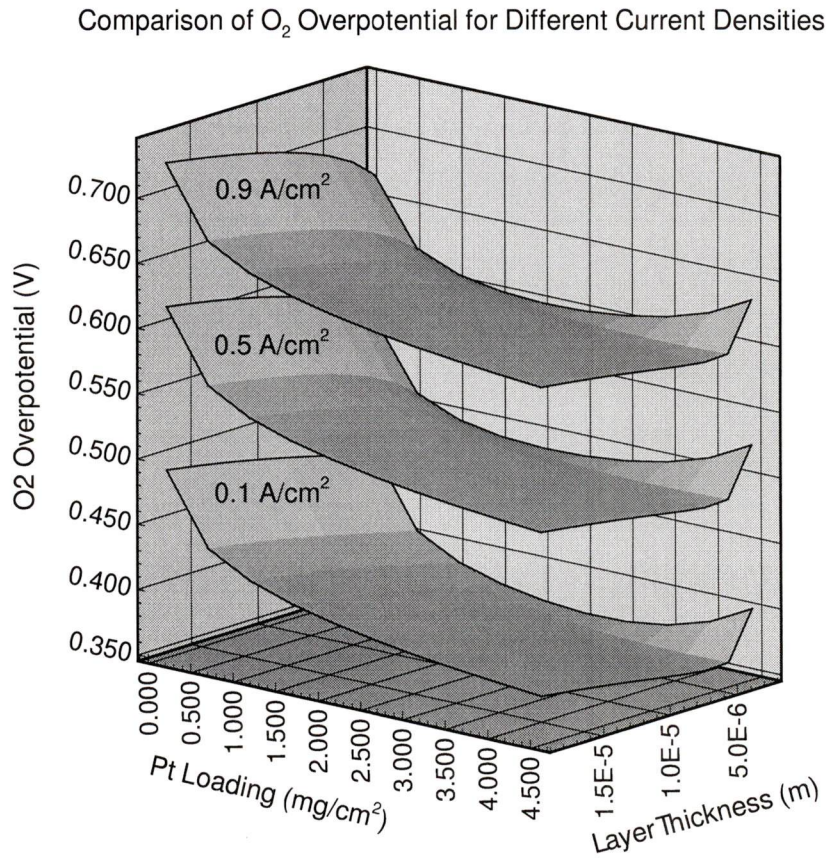

Figure 4.10: Effect of current density on the cathodic overpotential for Pt Black

for current densities 0.1, 0.5 and 0.9 A/cm^2. Although the cathodic overpotential changes, the relative difference between overpotential surfaces seems fairly constant. This indicates that there are no optimal current densities for a set configuration of catalyst layer. In other words, it makes no difference what current density the cell operates at, because any current density will yield the same relative change for that particular configuration of catalyst layer. This indicates that the design point for a PEM cell is practically independent of the current density.

Catalyst	load range (mg/cm^2)	thickness range (μm)
80%	.8-4.0	10-30
60%	.4-2.0	10-30
40%	.2-1.0	10-30
20%	0.05-.5	10-30

Catalyst Types and Optimal Loading

The effect of different catalysts on optimal loadings was also investigated. To determine the effects of different types of supported catalyst, a comparison of cathodic overpotential at 0.1 A/cm^2 was made. The loading and catalyst layer thickness ranges are given in Table 4.3.1.

The surfaces were plotted together and are shown in fig. 4.11. There are some interesting points to be made. First, it appears that the more surface area/load, the more sensitive the layer is to changes in composition. The 20% Pt surface curve is much sharper than the 80% surface. This indicates a higher sensitivity to mass transport, possibly because the active surface area increases more significantly for low percentage supported Pt than for high percantage supported Pt as Pt loading is increased. Hence, the overpotential η decreases faster for low percentage supported Pt. However for low percentage supported Pt, the solid volume increases faster. Thus mass transfer limitations increase faster as well.

Second, it is interesting to observe that there appears to be an optimum surface area for a supported catalyst. In this plot, the 40% supported catalyst appears to give much better performance than the 20% supported catalyst. This is surprising because one would expect a higher surface area to give a lower overpotential. However, because of mass transport limitations, the high surface area catalyst quickly depletes the oxygen. The lower surface area catalysts do not have this problem, and cut off

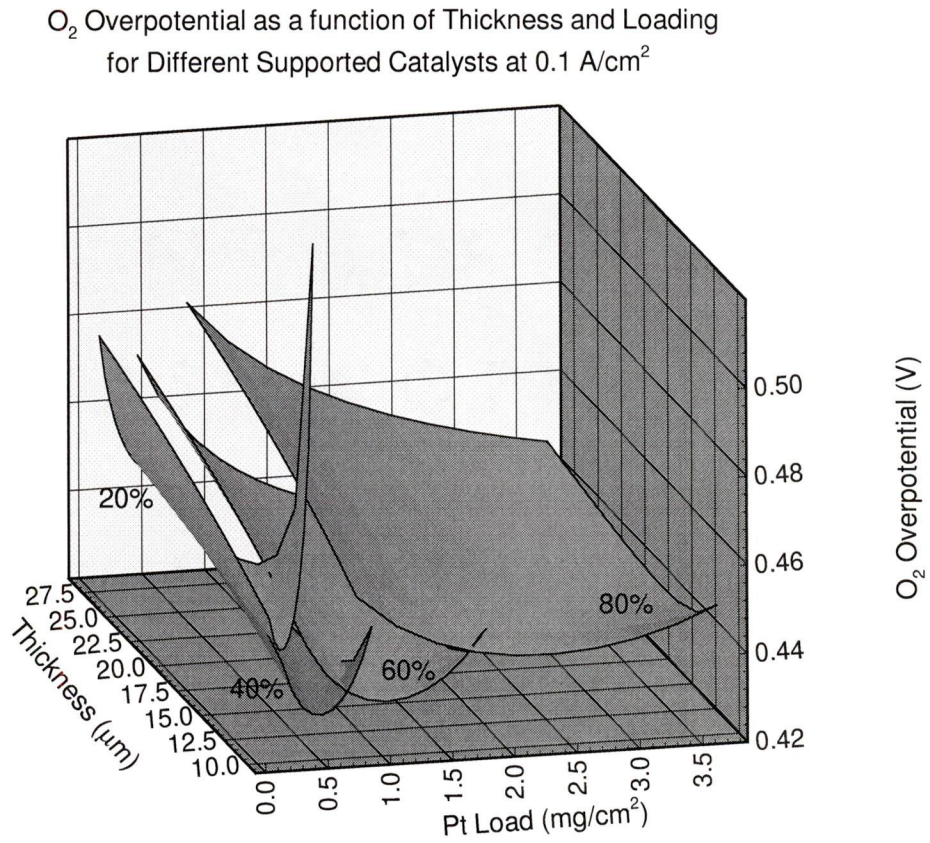

Figure 4.11: Supported Catalysts and their effect on cathodic overpotential at 0.1 A/cm^2

much more slowly. This indicates that there may be an optimal surface area density for catalyst layers.

An additional plot for 0.5 A/cm^2 was also done with the following values for catalyst loading. Ranges for catalyst loading and catalyst layer thickness are given in Table 4.3.1. Figure 4.12 shows the difference in the overpotential at higher current density. As seen from the plot, the optimum values do not change significantly, but the sensitivity of the O_2 overpotential does.

Catalyst	load range (mg/cm^2)	thickness range (μm)
80%	0.8-4.0	10-30
60%	0.4-2.0	10-30
40%	0.2-1.0	10-30
20%	0.05-.35	10-30

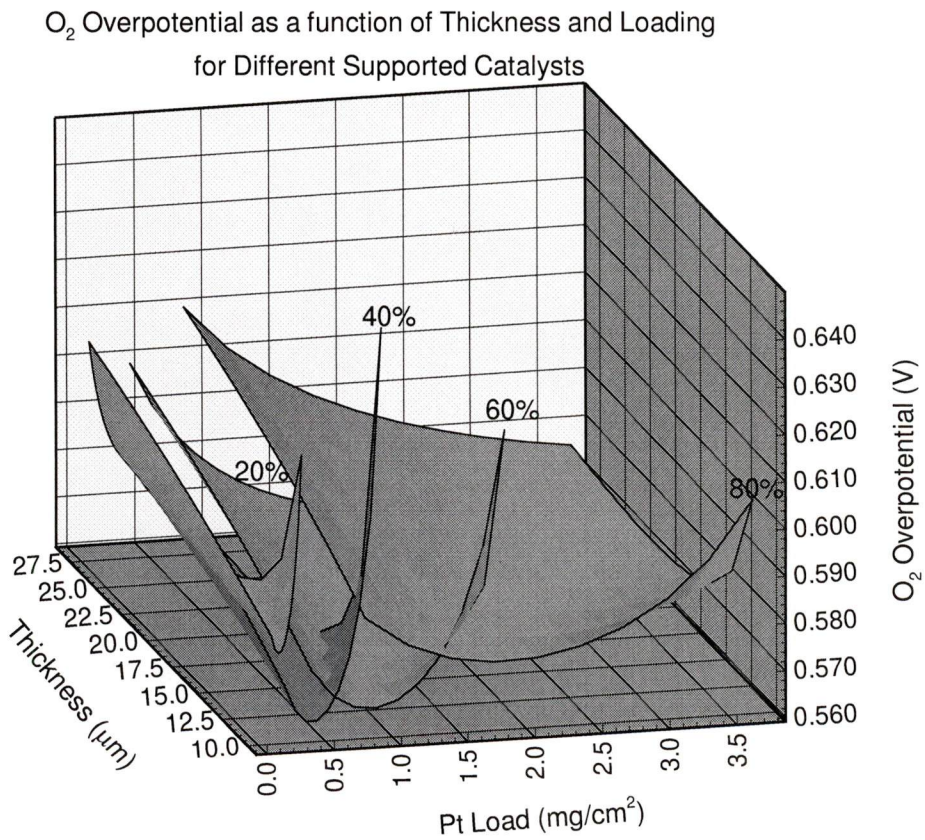

Figure 4.12: Supported Catalysts and their effect on cathodic overpotential at 0.5 A/cm^2

Porosity and Optimal Loading

The effect of porosity was also investicated to determine the existence of optimal loading points. The optimal void fraction was determined with a Golden Section method. With void fraction, plots indicated that the optimal loading occurred with a void fraction of 0.60. Three current densities (0.1, 0.5 and 0.9 A/cm^2) were investigated and all three showed an optimum void fraction of 0.60. This optimum void fraction of 0.60 is consistent with recent experimental observations by a research group in Germany [39] which indicated that electrodes with a catalyst layer void fraction of 65% showed the best performance.

The same optimisation test was done for different catalyst types. Again, there was no change in the optimal void fraction for performance. This indicates that a void fraction of 0.60 will give optimal performance and that the void fraction optimum appears to be insensitive to catalyst type and current densities.

The same plot was tried for a pure water layer, and a pure Nafion layer. This was done by using the bulk diffusion coefficient for the required material. Again, the result is surprising, showing that the optimum void fraction is at 60% for both materials. This constant optimal void fraction may be occurring because the optimum may not be sensitive to diffusion coefficient for the ranges that were tested.

To determine whether the void fraction optimum was independent of loading or current density, a plot of void fraction against current density and load was done. The results indicate that optimum void fraction is independent of both current density and catalyst load. The optimum value appears to be approximated 0.60. While this result is counter-intuitive, it may be explained as follows. First, the optimum void fraction may be relatively insensitive to changes in current density and loading for the ranges that were investigated. Second, the occurrence of the same optimal

void fraction value may be because the catalyst layer becomes mass transport limited at that condition.

This is more difficult to explain. In a mass transport limited case, the overpotential is set by the amount of catalyst that can react. This is determined by the diffusion coefficient. If the void fraction is set first, and the thickness determined after, then layers of varying loads will have the same overall void fraction and surface area corrections, but will differ by thickness of the layer. If both layers are operated at current densities that make them mass transport limited, then the effective thickness will be determined by the diffusion coefficient, and consequently the void fraction. Assuming the same void fraction, they will have the same effective thickness, and therefore, the same overpotential. Thus, the optimum void fraction will not change if the layer becomes mass transport limited.

4.4 Summary

Catalyst layer analysis with the present model indicates that catalyst is not being effectively used. As current density increases, the amount of Pt being used decreases. This indicates that Pt loads can be reduced for higher operating current densities.

Analysis of the catalyst layer confirms Weisbrod's identification of an optimum load for a catalyst layer thickness. Tests with different types of catalysts predicted that the 40% supported Pt would have the lowest overpotential.

Investigation into the optimal void fraction predicted a value of 60% void space would give the lowest overpotential. This value seems to be independent of both current density (0-1.0 A/cm^2) and catalyst type (Pt black, 20%-80%) for the range investigated.

Chapter 5

Conclusions and Recommendations

This thesis presented a performance model for a single proton exchange membrane fuel cell. While previous models had strong points, overall, there was not a model that was entirely suitable for use. This model takes the membrane model of Bernardi and Verbrugge and combines it with the catalyst layer model used by Weisbrod et al. The plug flow assumption was replaced with engineering approximations for channel flow, and additional equations were derived for ohmic resistance in the electrode and plate. The Stephan - Maxwell equation for gas diffusion was replaced with an approximation.

Overall, this model gives good qualitative predictions when compared with empirical data and previous models. Predictions by this model indicate that plate and electrode components with resistivities on the order of 10^{-3} will give inadequate performance. Because conducting polymers currently have resistivities in this range, they do not yet appear to be feasible materials for PEM cells.

Mass transport limitations effectively waste a portion of the catalyst. This portion increases as current density increases. Because Pt is not being effectively used at high current densities, it may be possible to reduce the amount of Pt in the cell. The model predicts that reduced loading will lower the performance at low current densities, but will have no effect at high current densities.

Investigations into the catalyst layer yielded some interesting results. First, mass transport is a significant factor in cell performance. This indicates that there will be limitations on the active surface area of the catalyst. This model predicts that a 40% supported catalyst will give the best performance of the supported catalysts.

Both performance optimisation and effective Pt usage are highly dependent on the composition of the layer. Investigations into optimal void fraction showed that a void fraction of 60% consistently gave the lowest cathodic overpotential. This value appears to be insensitive to both current density and catalyst type.

Recommendations

- The model is unverified experimentally. While trends and optimums are predicted, it is necessary to quantify these predictions with experimental results.
- The model is isothermal. Because the electrochemical reaction is temperature dependent, it would be advantageous to add models for heat transfer within the catalyst layer.
- The model uses one dimensional equations. Because much of the cell does not operate under constant conditions, expansion of the formulation to two and possibly three dimensions would give insight into enhancing performance through mass transport.
- The membrane model is too complicated for the present requirements and not complicated enough for addition of water transport models. Should the overall

model remain as is, a switch to a simpler, more empirical model would ease computational and intellectual requirements. The membrane model is not suitable in its present form for modelling any water transport. It must be reformulated to account for dry spots and changing osmotic drag with respect to membrane hydration.

- If conducting polymers are to be investigated, it is essential to develop a more accurate model for the electrode. The present model is meant only as a first run approximation, and will not give adequate results for electrodes with lower conductivities. To improve the electrode model, the following adjustments should be made:
  - account for the non-isotropic nature of the electrode if graphite is used
  - determine the current distribution in the channel
  - develop a correlation linking aspect ratio to the current distribution
- Hydrogen optimisation was not investigated in this model. However, because the hydrogen side has a faster reaction and higher mass diffusion, there is great potential to reduce the platinum loading on this side. If this is to be done, a model for catalyst layer poisoning by CO should be implemented if hydrocarbon reformed gas H_2 is to be used instead of pure H_2.

Appendix A

Computational Implementation

The computer model was written in C^{++} on a Sparc-20 using Unix as the operating system. The hardware and operating system were chosen because they offered more computational power than a personal computer. C^{++} was used as the programming language for several reasons:

- code is easily portable to other platforms
- for large programs, C^{++} code is easier to maintain than FORTRAN
- GUI addons will be easier to implement, once the main code is written.
- C^{++} is currently being taught at this university. FORTRAN is slowly being phased out of both industrial and scientific use. Given the present environment, finding competent FORTRAN programmers will become more and more difficult in the future.

In general, implementation of the code required no numerical techniques because most of the functions used to model physical processes could be reduced to analytical

expressions. However, the catalyst layer model consists of three first order equations that cannot be solved analytically.

The equations were implemented using a fourth order Runge-Kutta method and a shooting technique with a bisection algorithm. The Runge-Kutta routine was modified from original code provided by [40]. The values generated by this solver were checked with the differential equation tool in matlab. For the non-mass transport limited cases, both implementations converged to within 1% of each other.

Initially, long complex numerical solutions for any components were to be avoided. However, solving the catalyst layer equations using a SPARC-20 was reasonably fast. Further increases in speed are possible if the convergence criteria in mass transport limited areas is loosened and hydrogen catalyst layer calculations are removed. Because of the relative speed of the runs, this set of equations was integrated in the main model, rather than running several trials and approximating the behaviour with a set of correlations.

Further modifications were made to increase the accuracy of the effective catalyst layer thickness. One change involved increasing the solver variables from double to long double. Because of the increased overhead, the solution speed dropped significantly. No significant change in results was noticed, but this is because of a lack of an exponential function for long double operation and the fact that the compiler uses the same storage size for both doubles and long doubles. Currently, the numerical solver stores all variables as an RK_VAR type, which can be easily defined to the storage size that is needed. It would be useful to implement long doubles when an exponential function becomes available for that type and a larger storage value for long doubles is implemented with this compiler.

It is inherently difficult to estimate the location of the zero point because the Runge-Kutta solver cannot solve for cases where a zero concentration point occurs.

This occurs because the zero point also requires that the slope of the curve equals zero. The Runge-Kutta technique integrates the difference between an initial point and its projected derivative at the next point. As the value of this difference gets smaller, the solution becomes less stable. Because the solution converges asymtotically towards zero, the slope of the solution must equal zero as well.

The longer this near zero slope condition lasts, the more inaccurate the solution becomes. This is further complicated by the exponential nature of the equations. Thus, the solution becomes very sensitive to small changes in the initial guess as mass transport limitations increase because these limitations lengthen the near zero slope region. Figure A.1 shows the effect of changing the solution by less than one millionth of a volt. This small change causes large fluctuations and consequently, unreliable results. These fluctuations lessen as the low slope region decreases.

Because of this difficulty, any solution where the slope is zero is not easily solved. Consequently, cases where mass transport limitations exceed the desired current density will have unstable solutions. To solve for the mass transport limited cases, the zero point must be calculated indirectly. The program continually tries solutions with varying thicknesses of catalyst layer until the concentration at the edge of layer is within a threshold close to zero. This iterative guessing technique is implemented with a bisection algorithm.

Using a bisection algorithm, the solution gets smoother as the convergence criteria is decreased. As shown in Fig. A.2 , the limit is attained at around 1×10^{-9}. Too small of a criteria, say, 1×10^{-15}, causes numerical truncation errors to accumulate in the solution.

Figure A.3 shows a converged solution for a 5 μm thick catalyst layer. As seen from the plot, this technique works well. Although the solution is still quite rough, the general trend is easily seen.

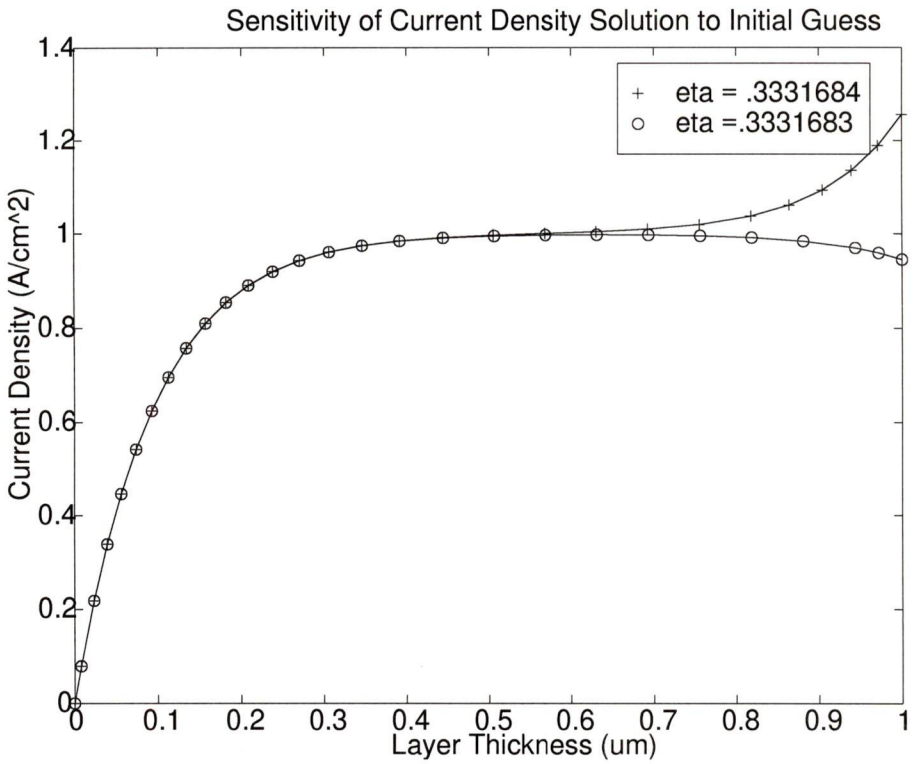

Figure A.1: Sensitivity of solution to very small changes in the initial guess of the cathode overpotential

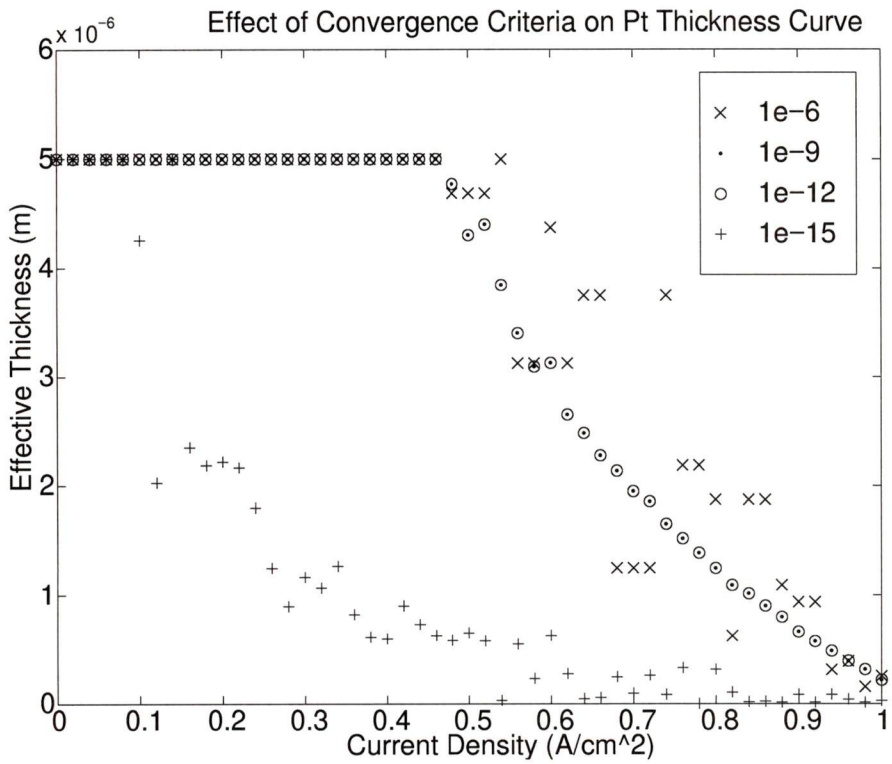

Figure A.2: Effect of convergence criteria on solution

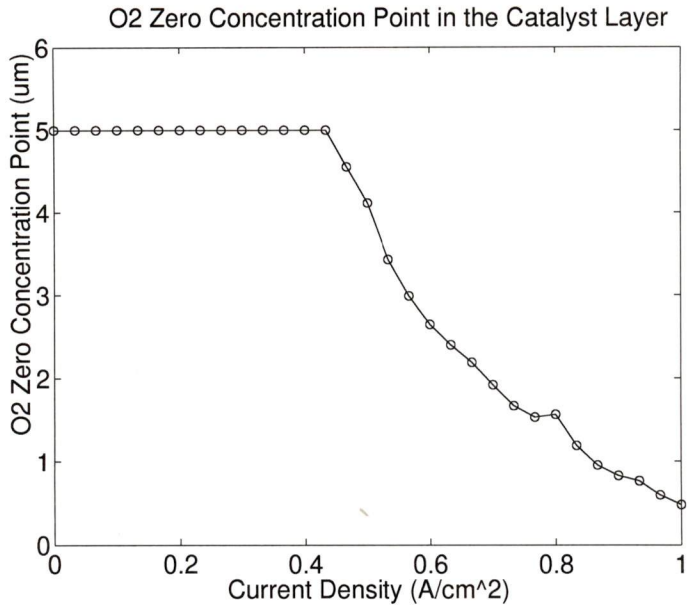

Figure A.3: Location of zero O_2 concentration in the catalyst layer as a function of current density

The roughness in the solution is likely due to truncation errors in the solution. Because the exponential nature of the formulation causes large changes for small perturbations, it seems reasonable that the slight oscillations are due to round off errors that change the last digit of the estimate, subsequently causing a large change in the solution. Attempts to smooth the solution with a second order extrapolation technique did not improve the results. This is most likely due to the flatness of the O_2 concentration curve. This would cause difficulties in extrapolation because the low slope will cause a large variation in the extrapolated value.

References

[1] Task Force on Cleaner Vehicles and Fuels. Report to Canadian Council of Ministers of the Environment, October 1995.

[2] Ministry of Environment Lands and Parks B.C. Clean Vehicles and Fuels for B.C., April 1995.

[3] A.J. Appleby and F.R. Foulkes. *Fuel Cell Handbook.* Kreiger Publishing, Malabar, Florida, 1989.

[4] ed. Leo J.M.J. Blomen and Michael N. Mugerwa. *Fuel Cell Systems.* Plenum Press, New York, 1993.

[5] Keith B. Prater. Solid Polymer Fuel Cell Developments at Ballard. *Journal of Power Sources*, 37:181–188, 1992.

[6] Daimler Benz. *High Tech Report*, March 1996.

[7] Junbom Kim, Seong-Min Lee, and Supramanian Srinivasan. Modeling of Proton Exchange Membrane Fuel Cell Performance with an Empirical equation. *J. ElectroChem. Soc.*, 142(8):2670–2674, 1995.

[8] J.C. Amphlett, R.M Baumert, R.F. Mann, B.A. Peppley, and P. R. Roberge. Performance Modeling of the Ballard Mark IV Slid Polymer Electroyte Fuel Cell. *J. ElectroChem. Soc.*, 142(1):1–8, 1995.

[9] J.C. Amphlett, R.M Baumert, R.F. Mann, B.A. Peppley, and P. R. Roberge. An Optimal Experimental Design for Fuel Cell Modelling. In *Fuel Cell Seminar: Programs and Abstracts*, pages 1550–1561, 1994.

[10] R.M. Baumert. Performance Modelling of the Ballard Mark IV Solid Polymer Electrolyte Fuel Cell. Master's thesis, Queen's University, 1993.

[11] Trung V. Nguyen and Ralphe E. White. A Water and Heat Management Model for Proton Exchange Membrane Fuel Cells. *J. ElectroChem. Soc.*, 140(8):2178–2186, 1993.

[12] S.J. Ridge and R.E. White. Oxygen Reduction in a Proton Exchange Membrane Test Cell. *J. electroChem. Soc.*, 7:1902–1909, 1989.

[13] Dawn M. Bernardi and Mark W. Verbrugge. A Mathematical Model of a Gas Diffusion Electrode Bonded to a Polymer Electrolyte. *AIChE J.*, 37(9):1151–1162, 1991.

[14] Dawn M. Bernardi and Mark W. Verbrugge. A Mathematical Model of a Solid Polymer Electrolyte Fuel Cell. *J. ElectroChem. Soc.*, 139(9):2477–2491, 1992.

[15] T.E. Springer, T.A. Zawodzinski, and S. Gottesfeld. Polymer Electrolyte Fuel Cell Model. *J. ElectroChem. Soc.*, 138(8):2334–2342, 1991.

[16] T.E. Springer, M.S. Wilson, and S. Gottesfeld. Modeling and Experimental Diagnostics in Polymer Electrolyte Fuel Cells. *J. ElectroChem. Soc.*, 140(12):3513–3526, 1993.

[17] Arvind Parthasarthy, Supramanian Srinivasan, and John Appleby. Pressure Dependence of the Electrode Kinetics of Oxygen Reduction at the Platinum/Nafion Interface - A Microelectrode Investigation. *J. ElectroChem. Soc.*, 139(10):2856–2862, 1992.

[18] Kirk R. Weisbrod, Steve A. Grot, and Nicholas E Vanderborgh. Through-the-Electrode Model of a Proton Exchange Membrane Fuel Cell. *Electrochemical Society Proceedings*, 23:153–167, 1995.

[19] Allen J. Bard and Larry R. Faulkner. *Electrochemical Methods: Fundamentals and Applications.* John Wiley and Sons, New York, 1980.

[20] J. A. Harrison and Z. A. Khan. The Oxidation of Hydrogen. *Journal of Electro-Analytical Chemistry*, 30(9):327–332, 1971.

[21] W. Vogel, J. Lindquist, P.Ross, and P. Stonehart. The Rate Controlling Setup for Electrochemical Oxidation of Hydrogen on Pt in Acid and Poisoning of the Reaction by CO. *Electrochimica Acta*, 20:79–88, 1975.

[22] Kim Kinoshita. *Electrochemical Oxygen Technology.* John Wiley and Sons, New York, 1992.

[23] Arvind Parthasarthy, Supramanian Srinivasan, and John Appleby. Temperature Dependence of the Electrode Kinetics of Oxygen Reduction at the Platinum/Nafion Interface - A Microelectrode Investigation. *J. Electrochem. Soc.*, 139(9):2530–2537, 1992.

[24] E-TEK, Inc. *Gas Diffusion Electrodes and Catalyst Materials, 1995 Catalogue*, 1995.

[25] Robert C. Reid, Joh M. Prausnitz, and Thomas K. Sherwood. *The Properties of Liquids and Gases.* McGraw-Hill, New York, 1977.

[26] Frank M. White. *Fluid Mechanics.* McGraw-Hill, New York, 1994.

[27] Robert E. De la Rue and Charles W. Tobias. On the Conductivity of Dispersions. *J. ElectroChem. Soc.*, 106:827–833, 1959.

[28] Ballard Power Systems. Personal communication, April 1996.

[29] Dawn M. Bernardi and Mark W. Verbrugge. Mathematical Model of Solid Polymer Electrolyte Fuel Cell. In *Proc. Symp. Model Batteries and Fuel Cells*, 1991.

[30] Frank P. Incropera and David P. De Witt. *Fundamentals of Heat and Mass Transfer.* John Wiley and Sons, New York, 1990.

[31] Forman A. Williams. *Combustion Theory : The Fundamental Theory of Chemically Reacting Flow Systems.* Princeton University, 1985.

[32] Sadik Kakac, Ramesh K. Shah, and Win Aung. *Handbook of Single-Phase Convective Heat Transfer.* John Wiley and Sons, New York, 1987.

[33] M.Necati Ozisik. *Heat Transfer: A Basic Approach.* Mcgraw Hill, Inc., New York, 1985.

[34] Jerry B. Marion and William F. Hornyak. *Physics for Science and Engineering.* Saunders College Publishing, New York, 1982.

[35] A. Murty Kanury. *Introduction to Combustion Phenomena.* Gordon and Breach, New York, 1975.

[36] Frank M. White. *Viscous Flow.* McGraw-Hill, New York, 1991.

[37] Ballard Power Systems. *The Ballard Fuel Cell: an Overview.*

[38] Ballard Power Systems. *Fuel Cell Operating Guidelines and Fuel Cell Performance Variables (Dow).*

[39] A. Fischer, Z. Veziridis, and H. Wendt. Comparing Different Production Technologies for Proton Exchange Membrane Fuel Cells. In *Proceedings of the 11th World Hydrogen Energy Conference*, 1996.

[40] William H. Press. *Numerical Recipes in C.* Cambridge University Press, New York, 1988.

VITA

Surname: Marr | Given Names: Curtis Lincoln

Place of Birth: Canada | Date of Birth: 04 July 65

Educational Institutions Attended:

University of Victoria	1985 to 1989
Capilano College	1983 to 1985

Degrees Awarded:

B.Eng.	University of Victoria	1989

PARTIAL COPYRIGHT LICENSE

I hereby grant the right to lend my thesis to users of the University of Victoria Library, and to make single copies only for such users or in response to a request from the Library of any other university, or similar institution, on its behalf or for one of its users. I further agree that permission for extensive copying of this thesis for scholarly purposes may be granted by me or a member of the University designated by me. It is understood that copying or publication of this thesis for financial gain shall not be allowed without my written permission.

Title of Thesis:

Performance Modelling of a Proton Exchange Membrane Fuel Cell

Author: [redacted]

Curtis Lincoln Marr

DEC. 19, 1996

Date